

Geochemical and isotopic insights into the assembly, evolution and disruption of a magmatic plumbing system before and after a cataclysmic caldera-collapse eruption at Ischia volcano (Italy)

R.J. Brown¹, L. Civetta^{2,3*}, I. Arienzo⁴, M.D'Antonio^{2,4}, R. Moretti^{4,5,6}, G. Orsi^{2,7}, E.L. Tomlinson⁸, P.G. Albert⁹, M.A. Menzies⁹

¹Department of Earth Sciences, Science Labs, Durham University, Durham, DH1 3LE, UK

²Dipartimento di Scienze della Terra, dell'Ambiente e delle Risorse, Università degli Studi di Napoli Federico II, Largo S. Marcellino, 80138 Napoli, Italy

³Istituto Nazionale di Geofisica e Vulcanologia, Sezione di Palermo, Via Ugo La Malfa 153, 90146 Palermo, Italy

⁴Istituto Nazionale di Geofisica e Vulcanologia, Sezione di Napoli-Osservatorio Vesuviano, Via Diocleziano 328, 80124 Napoli, Italy

⁵Dipartimento di Ingegneria Civile, Design, Edilizia e Ambiente, Seconda Università di Napoli, Via Roma 29, 81031 Aversa (CE), Italy

⁶Department of Geology, Saint Mary's University 923 Robie Street, Halifax, Nova Scotia, Canada.

⁷Dipartimento di Fisica "E. R. Caianiello" Università degli Studi di Salerno, Via Giovanni Paolo II 132, 84084 Fisciano, Salerno, Italy

⁸Department of Geology, Trinity College Dublin, College Green, Dublin, Ireland

⁹Department of Earth Sciences, Royal Holloway University of London, Egham Hill, Egham, Surrey TW20 0EX, United Kingdom

*email: richard.brown3@durham.ac.uk

Abstract

New geochemical and isotopic data on volcanic rocks spanning the period ~75–50 ka BP on Ischia volcano, Italy, shed light on the evolution of the magmatic system before and after the catastrophic, caldera-forming Monte Epomeo Green Tuff eruption (MEGT). Volcanic activity during this period was influenced by a

large, composite and differentiating magmatic system, replenished several times with isotopically distinct magmas of deep provenance. Chemical and isotopic variations highlight that the pre-MEGT eruptions were fed by trachytic/phonolitic magmas from an isotopically zoned reservoir that were poorly enriched in radiogenic Sr and became progressively less radiogenic with time. Just prior to the MEGT eruption the magmatic system was recharged by an isotopically distinct magma, relatively more enriched in radiogenic Sr with respect to the previously erupted magmas. This second magma initially fed several SubPlinian explosive eruptions and later supplied the climactic, phonolitic-to-trachytic MEGT eruption(s). Isotopic data, together with erupted volume estimations obtained for MEGT eruption(s) indicate that $>5\text{-}10\text{ km}^3$ of this relatively enriched magma had accumulated in the Ischia plumbing system. Geochemical modelling indicates that it accumulated at shallow depths (4–6 km), over a period of ca. 20 ka. After the MEGT eruption, volcanic activity was fed by a new batch of less-differentiated (trachyte-latitude) magma that was slightly less enriched in radiogenic Sr. The geochemical and Sr-Nd isotopic variations through time reflect the upward flux of isotopically distinct magma batches, variably contaminated by Hercynian crust at 8–12 km depth. The deep-sourced latitic to trachytic magmas stalled at shallow depths (4–6 km depth), differentiated to phonolite through crystal fractionation and assimilation of a feldspar-rich mush, or ascended directly to the surface and erupted.

Keywords: Ischia volcano; magmatic plumbing system; radiogenic isotopes; geothermometry; feldspar assimilation; caldera collapse.

1. Introduction

Caldera-forming eruptions are amongst the most destructive natural phenomena on the planet and can catastrophically disperse huge volumes of fragmented magma across large areas in hours to days. Understanding the processes that control the genesis and evolution of the large-volume silicic magmatic systems that feed caldera-forming eruptions, as well as their fate, is important in terms of hazard assessment (Druitt et al. 2012; Cashman and Sparks 2013). In order to decipher these processes, geological, geochemical and petrological investigations of volcanic rocks emplaced before, during and after large caldera-forming eruptions are needed (e.g., Bachman and Bergantz 2008; Charlier et al. 2008; Charlier and Wilson 2010). These can help understand both the processes responsible for the temporal and spatial assembly of large magma bodies and the response of a magmatic plumbing system following its partial destruction. Numerous studies of this type have been carried out to establish the complexity of these magmatic systems, and the important roles that magma composition, temperature, crystallinity and magma mixing play in their evolution (e.g. Foden 1986; Bacon & Druitt 1988; Bachmann and Bergantz 2008, Charlier and Wilson 2010, Pabst et al. 2008). Nevertheless, the origin of large volumes of silicic magma and the relative roles of fractional crystallization of mantle-derived mafic magmas, crustal contamination and/or remelting of crustal intrusive bodies in their petrogenesis remains a matter of debate. Recent work has revealed the short geological timescales over which critical processes within magma chambers can operate (Burgisser and Bergantz 2011; Druitt et al. 2012).

This paper presents a detailed study of the mineralogy and trace, major and isotope geochemistry of the magmas erupted at Ischia volcano, Italy, before, during and after the catastrophic, caldera-forming Monte Epomeo Green Tuff (MEGT) eruption. Ischia has received relatively scant scientific attention compared to neighbouring Campi Flegrei and Vesuvius volcanoes. The aim is to establish the characteristics of the magmatic system prior to and after the caldera-forming eruption, and to investigate the processes that control the genesis and evolution of the voluminous silicic magmatic reservoir. The island of Ischia (Fig. 1) is an instructive place to investigate this because the stratigraphic sequence, spanning the most recent caldera-forming eruption (MEGT eruption; Vezzoli 1988), is well known (e.g., Brown et al. 2008), and both pre- and post-caldera volcanic deposits are exposed outside the caldera depression. We outline new geochemical and isotopic data on the volcanic succession of the 75–50 ka BP

period of activity and use this to illustrate how the Ischia magmatic system prepared for the caldera-forming eruption and how it started to recover. Geochemical modeling constrains the depth and history of the pre- and post-MEGT magmas that were contaminated by Hercynian continental crust at 8–12 km depth and changed in composition from latite to phonolite through fractional crystallization and assimilation of feldspar from a crystal mush at 4–6 km depth.

2. Geological and magmatic history of Ischia

Ischia, an island volcano located at the NW corner of the Gulf of Naples, Southern Italy, is a densely populated active resurgent caldera (Fig. 1). The oldest dated rocks on the island, 150 ka old, are poorly exposed along the southern coast, and comprise part of an ancient island, about which little is known. Geophysical data indicate that Ischia is the remnant of an older volcanic complex that extended to the west (Orsi et al. 1999; Bruno et al. 2002; Paoletti et al. 2013). Petrological studies (Rittmann and Gottini 1981; Di Girolamo et al. 1979, 1995; Poli et al. 1987; Ghiara et al., 1979; Crisci et al. 1989; Civetta et al. 1991; D'Antonio et al. 2007, 2013) show that Ischia belongs to the low K-Series (Appleton 1972). Its volcanic products range in composition from shoshonite to latite, trachyte and phonolite (most abundant), according to the Total Alkali vs. Silica (TAS) classification diagram (Le Maitre et al. 1989). Phenocryst assemblages include alkali-feldspar, plagioclase, biotite, salite, diopside and olivine as major phases, and apatite, sphene, titanomagnetite and alkali-amphibole as the most common accessory phases (depending on whole rock composition).

Since 150 ka BP, Ischia has experienced discontinuous volcanic activity (Gillot et al. 1982; Vezzoli 1988; Orsi et al. 1996; de Vita et al. 2006, 2010; Fig. 1). Between 150 and 75 ka BP, trachytic and phonolitic lavas, lava domes and pyroclastic rocks were erupted. Between 75 and 60 ka BP, explosive eruptions emplaced a succession of pumice fall deposits, block-and-ash flow deposits and ignimbrites (Forcella et al. 1982; Rosi et al. 1988; Vezzoli 1988; Brown et al. 2008). The last 55 ka of activity on the island have been divided into three magmatic cycles based on stratigraphical, geochronological, geochemical, and Sr isotopic data (Poli et al. 1989; Civetta et al. 1991). The first cycle (55–33 ka BP) started with the caldera-forming MEGT eruption. Several phases of caldera collapse may have occurred during this period (Brown et al. 2008; Sbrana et al. 2009), and a $\sim 10 \times 7$ km diameter caldera was formed

(Vezzoli 1988; Tibaldi and Vezzoli 1998). The start of the second cycle (28–18 ka BP) was marked by the arrival of magmas that were less enriched in radiogenic Sr and that progressively mixed with the residual, more radiogenic and more differentiated magma residue from the first cycle. This recharge event probably initiated block resurgence in the caldera (Civetta et al. 1991). The third cycle (10 000 BP–1302 AD) was characterized by the eruption of latitic to phonolitic magmas with a wide range of isotope compositions. Petrographical, geochemical and isotopic characteristics of the latites (the Molara, Vateliero, Cava Nocelle and Arso eruptions) erupted over the past 3 ka, suggest mingling and mixing among variably evolved, small magma batches and the incorporation of crystals inherited from previous eruptions (e.g., Civetta et al. 1991; Di Girolamo et al. 1995; Piochi et al. 1999; D'Antonio et al. 2013). Data from olivine-hosted melt inclusions (MIs) in latites require gas-melt equilibria between 3 and 18 km depth, suggesting the presence of both deep and shallow magma reservoirs (Moretti et al. 2013).

The genesis of Ischia magmas has been studied by Tonarini et al. (2004), D'Antonio et al. (2007, 2013) and Moretti et al. (2013). In particular Moretti et al. (2013) suggest that magma genesis occurs in a mantle wedge modified by CO₂-rich fluids produced by devolatilization of subducted terrigenous-pelagic metasediments of the Ionian oceanic lithosphere. These mantle-derived magmas, mostly propelled by CO₂-rich fluids, rose to mid-upper crustal levels, where they stagnated and differentiated, and were subsequently periodically tapped as distinct magma batches. The arrival of these magma batches at shallow depths (Civetta et al. 1991; Piochi et al. 1999, and references therein) resulted in alternating periods of resurgence, intense volcanic activity and quiescence (Orsi et al. 1991; 1996; de Vita et al. 2006). The Monte Epomeo resurgent block records a net uplift of >900 m over ~30 ka (see Vezzoli 1988; Orsi et al. 1991; Tibaldi and Vezzoli 1998). Repeated flank failures have occurred during uplift, resulting in numerous debris flows (Tibaldi and Vezzoli 2004; de Vita et al. 2006; Rapolla et al. 2010; Della Seta et al. 2012) that have built a large submarine debris apron. The present active volcanic state of the island is indicated by historical ground movements (Buchner et al. 1996), seismicity (e.g., the 1883 Casamicciola earthquake) and by fumaroles and thermal springs (see Caliro et al. 1999; Inguaggiato et al. 2000; Di Napoli et al. 2009, 2011, 2013).

3. Volcanology and stratigraphy of the analysed volcanic units

Samples in this study come from volcanic products erupted on Ischia between ~75 and 50 ka BP.

Stratigraphic and geologic data on these eruptive units, summarized in Figures 2 and 3, are given in detail by Brown et al. (2008). This period leads up to, and includes part of, the first cycle of post-MEGT volcanic activity on Ischia (Civetta et al. 1991). We chose to study this time span because it brackets the 55 ka BP MEGT eruption—the largest eruption recorded on the island. The volcanic products of this period outcrop in coastal sections on the southern half of the island, as well as on Procida and western Campi Flegrei (Fig. 1). The geological record of the pre-MEGT activity is dominated by the products of explosive volcanic eruptions and includes numerous pumice fall deposits, ash layers, thin ignimbrites and block-and-ash flow deposits (Sant'Angelo to Porticello Tephra, Fig. 2). Products of the MEGT eruption outcrop in the resurgent caldera block in the centre of the island, along the south coast, on Procida and on the mainland. At least two thick ignimbrites (>70 and >200 m thick, respectively) ponded in the caldera. They are separated by a metre of volcanoclastic sediments and may record two phases of subsidence. Extra-caldera deposits of the MEGT include a coarse-grained (Plinian) pumice fall deposit, a widespread lithic breccia, and a distal ignimbrite in south-west Campi Flegrei (see Brown et al. 2008). Post-MEGT volcanic activity included Plinian or Subplinian eruptions recorded by ignimbrites and pumice fall deposits (Capo Grosso, La Roia and Schiappone Tephra, Fig. 2, 3), and phreatomagmatic eruptions (e.g., the Chiummano maar eruption). Several large tuff ring-forming eruptions at ~45 ka BP (e.g., Citara eruptions, Vezzoli 1988) support the notion that caldera collapse increased the access of seawater to erupting magma.

Estimating the volumes of the eruptions during this period is difficult. Most of the deposits are only intermittently exposed along the south, east and west coastlines of Ischia and only a few are found on neighboring Procida and in Campi Flegrei. A large proportion of the erupted material was dispersed across the sea. Distal ash layers from the MEGT have been found more than 300 km away (Tomlinson et al. submitted, and references therein). The volume of the MEGT eruption can be estimated from the size of the caldera, which measures 10×7 km, and has a minimum average subsidence of 200 m. This suggests a volume of ~9–15 km³ of erupted magma.

The stratigraphic positions of samples analysed in this study are given in Figure 3 for eruptive units where more than three samples were taken. One sample was taken from each of the Mago and La

Roia Tephra pumice fall deposits, one from the Chiummano Tephra and two from the Porticello Tephra (one each from the bottom and top of the unit).

4. Analytical procedure

All collected samples are either composite pumices from individual layers or obsidian clasts. Each analyzed sample comprised ~ 500 g of pumice clasts which were similar in colour, texture and crystal content. All samples were washed in distilled water multiple times, each time checking for the presence of halite. After dechlorinating, the exteriors of pumice clasts were removed with a hand saw, washed again multiple times in distilled water, crushed to lapilli-size particles, then ground and homogenized in an agate mortar. Major and trace elements were analyzed at Centre de Recherches Pétrographiques et Géochimiques, Nancy (France). Powders were analyzed for major oxides and Sc by inductively coupled plasma–atomic emission spectrometry and for the remainder of trace elements by inductively coupled plasma–mass spectrometry (ICP–MS). Precision is variable: 1–5%, for major elements, with the exception of P (<10%); <5%, for trace element contents higher than 50 ppm; 5–10%, for trace element contents in the range 10–50 ppm, and 5–15%, for trace element contents in the range 1–10 ppm.

Table 1 reports major and trace elements contents of the majority of the collected samples. Due to the intense unavoidable alteration of some of MEGT samples only trace element data is used for plots and geochemical modelling. Sr and Nd isotopic compositions were determined by Thermal Ionization Mass Spectrometry at the Istituto Nazionale di Geofisica e Vulcanologia, Sezione di Napoli-Osservatorio Vesuviano, using a ThermoFinnigan Triton TI[®] multicollector mass spectrometer. 0.1 g of whole rock powders were leached with cold 6 N HCl for 10 min and with warm 6 N HCl for 10 min, then rinsed several times in pure MilliQ[®] water. Sr and Nd were separated by conventional ion-exchange chromatographic techniques. Due to the low Sr content of a large number of samples and to the clear evidence of the effects of seawater chemical alteration, for the majority of the samples, we have analysed ca. 0.1 g of feldspars. Mineral fractions were ultrasonically cleaned in diluted hydrofluoric acid (7%) and then rinsed with MilliQ[®] water, before dissolution. In few cases isotope analysis on different aliquots of mineral fractions were performed. Measured $^{87}\text{Sr}/^{86}\text{Sr}$ and $^{143}\text{Nd}/^{144}\text{Nd}$ isotope ratios were normalized for within-run isotopic fractionation to $^{86}\text{Sr}/^{88}\text{Sr}=0.1194$ and $^{146}\text{Nd}/^{144}\text{Nd}=0.7219$, respectively. Sr blanks were

on the order of less than 0.5 ng during the period of chemistry processing. The mean measured value of $^{87}\text{Sr}/^{86}\text{Sr}$ for NIST-SRM 987 and of $^{143}\text{Nd}/^{144}\text{Nd}$ for La Jolla, during the period of measurements, were 0.710204 ± 0.000015 (2σ , $N=72$) and 0.511834 ± 0.000009 (2σ , $N=32$), respectively. The external reproducibility 2σ is calculated according to Goldstein et al. (2003). Sr and Nd isotope ratios have been normalized to the recommended values of NIST SRM 987 ($^{87}\text{Sr}/^{86}\text{Sr}=0.71025$) and La Jolla ($^{143}\text{Nd}/^{144}\text{Nd}=0.51185$) standards, respectively. Sr and Nd isotope data for the 75–45 ka volcanic rocks and separated feldspars are reported in Table 1. Given the high Rb/Sr, the $^{87}\text{Sr}/^{86}\text{Sr}$ ratios measured on whole rocks have been corrected for ^{87}Rb decay since eruption. Major elements content of minerals used in modelling were determined by Electron Microprobe analyses. Details on the analytical procedures are in Di Napoli et al. (2013).

5. Results

5.1 Petrography

The investigated pre-MEGT and MEGT rocks are variably vesicular and porphyritic, with a total phenocryst content of pumice clasts in the range 5–25 vol%, whereas scoria, obsidian and lava clasts may reach 40 vol% (Table 2). Alkali-feldspar is the dominant phenocryst; some crystals reach 2–3 mm in diameter. Additional phenocrysts phases include clinopyroxene, plagioclase and black mica (in decreasing order of abundance): opaque oxide minerals, and apatite are common accessory phases. Alkali-feldspar varies from sanidine-Na-sanidine-anorthoclase; clinopyroxene is ferroan diopside with variable Fe content; plagioclase is andesine; black mica is ferrian phlogopite; and opaque oxide is Ti-magnetite. Reverse zoning is often observed in plagioclase and alkali-feldspar crystals, many of which are rounded and show textural signs of resorption and/or recrystallization.

The mineral assemblages vary according to the chemical composition of the rock. Trachytes are characterised by dominant alkali-feldspar, followed by clinopyroxene, plagioclase, ferrian phlogopite, opaque oxide and apatite; the groundmass is mostly glassy with rare microlites of alkali-feldspar and sometimes ferrian phlogopite and clinopyroxene, when optically resolvable. Phonolites are characterised by a rarity or absence of plagioclase, by dominant alkali-feldspar, very minor amounts of clinopyroxene, black mica and opaque oxide, and by additional phases such as alkali-amphibole, nepheline and sphene in a few

obsidian and lava samples. Of the latter mineral phases, sphene and alkali-amphibole occur as microphenocrysts or microlites, whereas nepheline is confined to the groundmass, along with abundant opaque oxides (Table 2). The occurrence of optically distinct alkali-feldspar overgrowths around alkali-feldspar phenocrysts may suggest mixing among magmas of variable composition (e.g., Ginibre and Wörner 2007).

Petrographic evidence for alteration occurs in some samples from these older units, particularly in the Sant'Angelo, Olummo and MEGT deposits.; carbonate as either patches in the groundmass, or as veins cross-cutting phenocrysts; partial or complete transformation of clinopyroxene into Fe-oxy-hydroxides and carbonate, and of ferrian phlogopite into chlorite. The groundmass glass of these altered samples is variably transformed in secondary clay minerals and/or analcite and carbonate. More information on the secondary mineralogy of MEGT rocks and their implications for the hydrothermal circulation at Ischia can be found in Di Napoli et al. (2013).

The petrographic features of post-MEGT rocks are similar to those of both pre-MEGT and MEGT rocks. However, post-MEGT rocks include few latites and trachytes (from Chiummano and Schiappone units). The latites are characterized by more abundant plagioclase and clinopyroxene, and rare alkali-feldspar and olivine phenocrysts with respect to the trachytes (Table 2).

5.2 Geochemistry and isotope geochemistry

We present new geochemical and isotopic data for volcanic rocks erupted on Ischia between ~75 and 50 ka BP. Figure 4 compares the new data with previously published geochemical data on Ischia volcanic rocks in a TAS plot. The analyzed volcanic products range in composition from latite to phonolite. In Figure 5 whole rock data of the analyzed samples are plotted together with fields encompassing major and trace element data acquired on glasses from the same samples (see Tomlinson et al. submitted). In these plots CaO content has been used as differentiation index. Analyses of pumice from an older ignimbrite (Barano ignimbrite, ~150 ka BP, Gillot et al., 1982) on the southeast coast of Ischia are included as a reference to the earlier magmatic history.

5.2.1 Pre-MEGT eruptions

The oldest eruption in the studied succession is recorded by Sant' Angelo Tephra: a >25 m-thick sequence of pumice fall deposits and thin ignimbrites capped by two block-and-ash flow deposits from a dome-forming eruption (Brown et al. 2008; Fig. 2). The eruption is thought to be of small volume, with the vent located ca.1 km from the outcrop on the Sant' Angelo peninsula (Fig.1). The composition of the Sant' Angelo magma (Figs. 5, 6) shows a slight variation through time from more- to less-differentiated phonolite, back up to more differentiated phonolite (CaO from ~1.1 up to 1.5 wt.%, then to ~1.0 wt.%; Zr from ~800 to 600 ppm, then up to ~1100 ppm). Most samples have a slight peralkalinity (Agpaitic Index, A.I.= molar (Na₂O+K₂O)/Al₂O₃=0.98-1.08, Table 1). The ⁸⁷Sr/⁸⁶Sr of Sant' Angelo feldspar phenocrysts is almost constant through the sequence (0.706557±6 -0.706642±6; hereafter, the quoted error refers to the last digit) (Fig. 6). ¹⁴³Nd/¹⁴⁴Nd ranges from 0.512547±6 to 0.512537±6, from the base of the stratigraphic section upward (Table 1).

The following eruptive unit is Mago Tephra. It is a poorly preserved <60 cm-thick pumice fall deposit comprised of fine- to medium-grained pumice lapilli. It is considered to have been a small eruption vented from somewhere in the centre of the island. Only one sample was analysed. Its CaO and Zr contents are ~1.0 wt.% and ~1000 ppm, respectively (Figs. 5, 6), indicating that the Mago magma (A.I.=~1.1) was compositionally similar to the last-erupted Sant' Angelo magma, but was slightly less enriched in radiogenic Sr (⁸⁷Sr/⁸⁶Sr=0.706537±6). Its ¹⁴³Nd/¹⁴⁴Nd is similar to that measured in the last erupted Sant' Angelo Tephra products (0.512536±5) (Table 1).

The Olummo Tephra is a 6 m-thick sequence of pumice fall deposits capped by a block-and-ash flow deposit. The Olummo magma shows a wide range of composition (Figs. 5, 6). Initially, a more differentiated phonolitic magma (CaO=~1.0 wt.%; Zr =~1100 ppm; A.I.=1.1) was erupted, similar to the Mago and to the last-erupted Sant' Angelo magmas. During the course of the Olummo eruption, magma composition changed to trachyte (CaO=~1.6 wt.%; Zr=~400 ppm; A.I.=0.9). ⁸⁷Sr/⁸⁶Sr isotope ratios of whole rock and separated feldspar phenocrysts gradually changed, during the course of the eruption, from 0.706569±6 to 0.706416±6, whilst ¹⁴³Nd/¹⁴⁴Nd remained unchanged for all the analysed samples (~0.51254) (Fig. 6; Table 1).

The > 7m-thick Tisichiello Tephra (76 ± 3 ka, based on correlation with the varved Lago Grande di Monticchio core, Tomlinson et al, submitted) reaches 7 m in thickness and comprises a complex

succession of pumice fall deposits and thin ignimbrites (Brown et al. 2008). It was potentially a larger-volume eruption than the preceding eruptions. The first-erupted Tisichiello magma is trachytic in composition (CaO \approx 1.7 wt.%; Zr \approx 400 ppm; A.I.=0.9) and compositionally and isotopically similar ($^{87}\text{Sr}/^{86}\text{Sr}$ = 0.706449 \pm 6; $^{143}\text{Nd}/^{144}\text{Nd}$ =0.512550 \pm 5) to the last-erupted Olummo magma (Fig. 6; Table 1). The late-erupted Tisichiello magma is phonolitic in composition (CaO \approx 1.1 wt.%; Zr \approx 950 ppm; A.I. =1.1), more radiogenic ($^{87}\text{Sr}/^{86}\text{Sr}$ =0.70687 \pm 6 -0.706732 \pm 6) and is separated from the first-erupted trachytic magma by a relative wide Sr isotopic gap. Its $^{143}\text{Nd}/^{144}\text{Nd}$ is lower than that of the trachytic Tisichiello magma (0.512536 \pm 6) (Table 1).

The last recorded eruption before MEGT is the >3.5 m-thick Porticello tephra (Brown et al. 2008) (59 \pm 2 ka, based on correlation with the varved Lago Grande di Monticchio core, Tomlinson et al., submitted), which is composed of <4 m of pumice fall deposits and thin ash layers. Products from this eruption are trachytic/phonolitic in composition (CaO \approx 1.1 wt.%; Zr \approx 600 ppm; A.I.=1.0) and have $^{87}\text{Sr}/^{86}\text{Sr}$ (0.706752 \pm 6-0.706784 \pm 6) in the range of those of the late products of the Tisichiello eruption. $^{143}\text{Nd}/^{144}\text{Nd}$ (0.512539 \pm 5) is similar, within the analytical errors, to the value characterizing the last erupted Tisichiello magma.

5.2.2 MEGT eruption

The 55 ka MEGT eruption was characterized by the emission of a variety of volcanic products ranging in composition from trachyte to phonolite. Early phases of the eruption are recorded outside the caldera by a 7 m-thick phonolitic to trachytic pumice fall deposit (CaO \approx 1.0 wt.%; Zr=800 to 700 ppm; A.I. \approx 1) overlain by a phonolitic welded ignimbrite (CaO \approx 1.1 wt.%; Zr =770 ppm; A.I. \approx 1; Figs. 3, 5, 6). This is overlain by lithic breccias considered to record a phase of caldera collapse. Pumice and dense glassy clasts in these breccias are of less differentiated trachytic/phonolitic composition (CaO \approx 1.5–1.1 wt.%; Zr \approx 350-650 ppm A.I. \approx 1). Intracaldera deposits comprise two thick ignimbrites. The lower ignimbrite has basal lithic breccias (see Fig. 3), and is compositionally similar (CaO \approx 1.2 wt.%; Zr \approx 370 ppm; A.I. \approx 0.9) to the lithic breccias exposed at the coast (Brown et al. 2008). The magma that fed the upper ignimbrite was less differentiated (Zr=150–210 ppm).

The first erupted MEGT magma ($^{87}\text{Sr}/^{86}\text{Sr}=0.706753\pm 8$, $^{143}\text{Nd}/^{144}\text{Nd}=0.512534\pm 5$) is isotopically similar to the Porticello magma and to the last-erupted Tisichiello magma. During the course of the MEGT eruption Sr isotopic composition varies from 0.706753 \pm 8 to 0.706907 \pm 6, while $^{143}\text{Nd}/^{144}\text{Nd}$ remains constant ($^{143}\text{Nd}/^{144}\text{Nd}\sim 0.512540$) (Table 1).

5.2.3 Post-MEGT eruptions

The >50 cm-thick La Roia Tephra is the first recorded eruption after the MEGT eruption (Brown et al. 2008). It comprises a 50 cm thick trachyte pumice fall deposit with Zr contents slightly higher than the last erupted MEGT magmas (CaO \sim 2.2 wt.%; Zr=290 ppm; A.I. \sim 0.9), but less enriched in radiogenic Sr ($^{87}\text{Sr}/^{86}\text{Sr} = 0.706732\pm 6$) (Figs. 5,6) than MEGT.

The Capo Grosso Tephra is a 40 m thick ignimbrite. The eruption tapped a trachytic magma (CaO \sim 2.7 wt.%; Zr=200 ppm; A.I. \sim 0.9) slightly less differentiated than the La Roia Tephra and characterized by $^{87}\text{Sr}/^{86}\text{Sr}$ of 0.706686 \pm 6, less enriched in radiogenic Sr than the last erupted MEGT and the La Roia magmas (Fig. 6; Table 1). The Chiummano Tephra, interpreted as the deposits of a maar eruption in the south of the island, records the extrusion of the least evolved magma of the studied period, having a latitic composition (CaO \sim 7.1 wt.%; Zr=130 ppm; A.I. \sim 0.7). Two different aliquots of separated feldspar have $^{87}\text{Sr}/^{86}\text{Sr}$ of 0.706668 \pm 7 and 0.706691 \pm 6, while the whole rock has $^{143}\text{Nd}/^{144}\text{Nd}$ of 0.512534 \pm 6 (Table 1). The Sr isotopes are similar to those measured for Capo Grosso rocks (Figs. 5, 6).

The youngest eruption in the studied period is the Schiappone Tephra (50.6 \pm 2 ka, based on correlation with the varved Lago Grande di Monticchio core; Tomlinson et al., submitted) whose products outcrop extensively along the south coast of Ischia (Brown et al 2008). It comprises a complex basal pumice fall deposit up to 6 m thick overlain by a >60 m thick ignimbrite. Pumice clasts within the middle part of the pumice fall deposit exhibit compositional banding and the bulk composition varies from trachyte to latite during the course of the eruption (CaO from 1.4 to 5 wt.%; Zr from 370 to 220 ppm; 0.8 <A.I.<0.9). All the erupted products are characterised by homogeneous Sr and Nd isotopic compositions ($^{87}\text{Sr}/^{86}\text{Sr} = 0.70674\text{--}79$; $^{143}\text{Nd}/^{144}\text{Nd}=0.512527\text{--}30$) higher than La Roja, Chiummano and Capo Grosso products.

5.2.4 Chemical and isotopic trends

Magmas feeding the pre-MEGT and MEGT eruptions were more differentiated (trachyte to phonolite) than those feeding the post-MEGT eruptions (latite to trachyte). With increasing degree of differentiation (decreasing CaO content; Figs. 5, 6), the data show that for the pre-MEGT magmas, SiO₂, Al₂O₃, K₂O first increase and then decrease; MnO, Zn, Y, Nb, Rb, Cs, Rare Earth Elements (REE) except Eu, and Th first remain constant and then increase; Na₂O increases, whereas MgO and P₂O₅ (and V, Sr, Ba, Eu) decrease; Fe₂O₃ and TiO₂ first decrease and then increase. The pre-MEGT rocks match well with the highly evolved MEGT magma for major and trace elements, but are less enriched in radiogenic Sr, with the exception of the last erupted Tisichiello and the Porticello magmas, both characterized by Sr isotope ratios similar to the first erupted MEGT magma (Fig. 6). The highly evolved pre-MEGT and MEGT rocks are characterized by significantly higher TiO₂, Fe₂O₃, P₂O₅ contents, compared to the post-MEGT rocks, for similar CaO content (Fig. 5). The post-MEGT magmas (latite to trachyte) display a wide range of composition (CaO from 7.0 to 1.5 wt.%, Zr from 128 to 365 ppm; Fig. 5). The content of many trace elements (e.g. Zr, REE, Th) well discriminates post-MEGT with respect to pre-MEGT and the most evolved MEGT products (Fig. 6).

In conclusion the 75–50 ka BP rocks show a wide range of ⁸⁷Sr/⁸⁶Sr (0.70642–0.70691). In particular, magmas extruded during the pre-MEGT eruptions show the widest ⁸⁷Sr/⁸⁶Sr range (0.70642–0.70688), whereas those erupted at the end of Tisichiello eruption and during the Porticello, MEGT and post-MEGT volcanic activity are characterized by a more restricted ⁸⁷Sr/⁸⁶Sr range (0.70667–0.70691). Nd isotope ratios show a more restricted range throughout the studied period (0.51253–0.51255), although significant with respect to the analytical error. They show a slightly negative correlation with Sr isotope ratios (Fig. 7).

6. Discussion

6.1 Geochemical modelling

The overall compositional variation displayed by the investigated rocks (e.g. Fig. 8a, b, c) can be attributed, on first approximation, to fractional crystallization processes from a less- to a more-evolved magma. This possibility has been explored by means of least-squared mass balance calculations (Stormer and Nicholls,

1978). Since Harker diagrams exhibit abrupt changes at CaO ca. 1.5 wt.%, two fractionation steps have been considered. For the first step, the composition of the Chiummano latite sample (OIS 0324) has been taken as parent magma. Modelling reveals that ca. 44 wt.% removal of a solid assemblage, made up of Mg-rich clinopyroxene, labradoritic plagioclase, biotite, Ti-magnetite and apatite (in decreasing order of abundance), leads to a trachytic daughter magma similar to the first-erupted Schiappone magma (sample MEGT 0312 in Tables 1 and 4) ($\sum r^2=0.25$; Fig. 8; Table 3). From the latter magma, a second step has been modelled, to reproduce the phonolitic composition of the TiO₂ rich-glass sample OIS 0329 (Table 4 and Tomlinson et al. submitted). By subtracting ca. 63 wt.% of a different mineralogical assemblage, constituted by dominant alkali-feldspar, and subordinate andesinic plagioclase and alkali-amphibole (Fig. 8; Table 3), the calculation accounts only in part for the increase in TiO₂ and F₂O_{3tot} contents, and the decrease in SiO₂ shown by the most evolved, phonolitic pre-MEGT magma (Fig. 8).

To further constrain the role of fractional crystallization from less- to more-evolved Ischia magmas, and to investigate the possible occurrence of concomitant open-system evolution processes, we used the MELTS code (Ghiorso and Sack, 1995; Asimow and Ghiorso, 1998; Smith and Asimow, 2005). In order to run the program properly, independent geothermobarometric constraints have been obtained by melt-crystal phase equilibria. In particular, by using the TiO₂ exchange between melt and biotite (Righter and Carmichael, 1996), we found that Ischia trachytes equilibrated at a temperature of 930°C. This value was obtained for both a TiO₂ (and Fe²⁺)-poor biotite, likely crystallized from a poorly-evolved trachyte magma, and a TiO₂ (and Fe²⁺)-rich biotite crystallized from a slightly more evolved trachyte, represented by samples MEGT 0308 and MEGT 0312, respectively (Table 4). In the evolving magma, at the obtained temperature, biotite records an increase in oxidation from $\log f_{O_2} = NNO + 0.75$ to $\log f_{O_2} = NNO + 1.5$, possibly accompanied by an increase of the population of OH⁻ groups in the X-site with respect to F⁻ and Cl⁻. Remarkably, by using the mica-sanidine-magnetite geothermobarometer, proposed by Wones and Eugster (1965) and recently re-calibrated and applied to Campi Flegrei rocks (Fabbrizio et al. 2009), we again obtain a temperature of 930°C (Table 4). The estimated temperature (as well as the obtained $\log f_{O_2}$) can be used by adopting the solubility model of Papale et al. (2006) to retrieve information about the water content under which Ischia magmas evolved. Dissolved H₂O contents calculated for $\log f_{O_2} = NNO + 0.75$

and $\log f_{\text{O}_2} = \text{NNO} + 1.5$ are 2.92 wt.% (sample MEGT 0308) and 2.40 wt% (sample MEGT 0312), respectively.

If fugacities are approximated to partial pressures (disregarding the presence of CO_2 in the system), and a crustal density of 2500 kg/m^3 is assumed (P. Capuano personal communication) then the calculated H_2O contents correspond to depths of 2–4 km (52–100 MPa). If we consider the occurrence of dissolved CO_2 in magmas, besides H_2O contents, and assume as CO_2 contents the background degassing conditions of the Ischia magmas (Moretti et al. 2013), then the storage depths increase to 4–6 km (100–160 MPa). This depth range is in line with both estimates of major storage regions within the Ischia magmatic plumbing system based on geophysical modeling (Orsi et al. 1999; Paoletti et al. 2009; 2013), and recent MI data (Sbrana et al. 2009; Moretti et al. 2013). It also corresponds to the depths of magmas feeding the adjacent Campi Flegrei caldera (e.g., Mangiacapra et al. 2008; Arienzo et al. 2010, and references therein). Henceforth, for calculations relative to trachytic magmas we will use an average pressure value of 130 MPa corresponding to depths of ~5 km. Barometric estimates based on MIs data (Moretti et al. 2013) and geophysical data (Orsi et al. 1999) further suggest the existence of a deeper, less-differentiated magmatic reservoir at 8–12 km depth, partially corresponding to the 8-10 km deep magmatic sill revealed by seismic tomography at Campi Flegrei and Vesuvio (Auger et al. 2001; Zollo et al. 2008) and constrained by MIs studies (e.g. Mangiacapra et al. 2008; Arienzo et al. 2010).

For MELTS calculations (see Appendix), we used the Chiummano latite (sample OIS 0324; Table 4) as a starting composition. For such a poorly differentiated magma we assumed as initial P and T 200 MPa and 1200°C , respectively, in agreement with current knowledge of magma storage at 8–12 km depths (Orsi et al. 1999; Moretti et al. 2013). The first modeled step of magma differentiation ends at 130 MPa (ca. 5 km depth). At such a pressure the residual liquid (72%) reaches a composition close to that of the poorly evolved trachyte (sample MEGT 0308; Fig. 8; Table 4). From this point on, by using the MELTS code, it is practically impossible to reach the composition of the more evolved Schiappone trachyte (sample MEGT 0312) by fractional crystallization (either by changing f_{O_2} and/or water content), i.e., it cannot generate a melt with the high SiO_2 and Al_2O_3 values detected in the natural sample (~62.6 and ~18.9 wt.%, respectively; Table 4). On the contrary, the system evolves towards more under-saturated compositions. MELTS code is calibrated for mafic systems and performs well for MORBS and alkalic mafic magmas.

Despite that, it is possible to partially fill the compositional gap between the less evolved (sample MEGT 0308) and the more evolved (sample MEGT 0312) Schiappone trachyte (Fig. 8) by modeling isothermal-isobaric assimilation of felsic rocks (as suggested by geochemical modeling results, reported in the previous section) and still keeping active the fractional crystallization function (Appendix). The felsic rocks used for this purpose are feldspars crystallized from earlier magmas. In fact, only feldspars have $\text{SiO}_2/\text{Al}_2\text{O}_3$ ratios that are comparable with that of the evolved trachyte. Results are reported in Table 4 (MELTS step 2). The occurrence of such a process can be inferred by petrographic investigations (rounded or recrystallized feldspar crystals and reversely-zoned plagioclase and feldspar compositions). A similar process has been suggested recently for the Teide-Pico Vejo complex (Tenerife, Canary islands; Wiesmaier et al. 2012) for which the evolved phonolite magmas are interpreted as the result of AFC involving nepheline-syenites from previous eruptions.

Fractional crystallization driven by decompression allows magma that is compositionally similar to the Schiappone sample MEGT 0312 to evolve further and reach a composition similar to that of the pre-MEGT phonolitic magmas. During this decompression stage, Fe_2O_3 , TiO_2 , Na_2O and MnO increase, SiO_2 decreases, while CaO remains approximately constant or slightly decreases. Results, summarized in Table 4 (Melts Step 3 and 4), corroborate the hypothesis that feldspar assimilation may represent an essential step to give rise to a compositional lineage extending from latite to phonolite in volcanic systems fed by evolved alkaline magmas. In such systems, the occurrence at depth of large amounts of feldspar-rich cumulates left by earlier eruptions, as inferred on volcanological and petrological grounds for the Campi Flegrei caldera (D'Antonio 2011), makes the process of extensive assimilation of such material very likely to occur.

6.2 Isotopic modelling

We modeled the effects of crustal contamination on latitic magma to reproduce the overall compositional and isotopic range displayed by the 75–50 ka BP volcanic rocks, in line with that recently proposed for Campi Flegrei magmas (e.g. D'Antonio et al. 2007; Di Renzo et al. 2011; Arienzo et al. 2011). We used the EC-AFC (Energy Constrained Assimilation and Fractional Crystallization) model of Spera and Bohrsen (2001), and assumed that the latitic magma ascended to a depth of 8–12 km, where it was contaminated by continental crust. Results of the modeling are plotted as a blue curve in Figure 7, and the parameters used

are listed in Table 5. We assigned to the parental magma the composition of the Chiummano latite, and the Sr and Nd isotope compositions of the least radiogenic Tischiello magma (Table 1). The average composition of the Hercynian continental crust of the Calabrian region was used as an assimilant (Rottura et al. 1991). The contamination: 1) increases the $^{87}\text{Sr}/^{86}\text{Sr}$ ratio; 2) decreases the $^{143}\text{Nd}/^{144}\text{Nd}$ ratio, and 3) decreases magma temperature from 1250 to 1096°C. Both temperature values are in line with temperature ranges for latitic melts (e.g. Cannatelli et al. 2007) and with MELTS simulations (see above). At such T values, the modeled daughter magma has geochemical and Sr isotopic compositions close to that of the trachytic Schiappone magma.

6.3 Magmatic evolution through time

The slight compositional variation exhibited by the Sant'Angelo magmas through time (from more-differentiated to less-differentiated phonolite, back up to more-differentiated phonolite) coupled with a quasi-constant $^{87}\text{Sr}/^{86}\text{Sr}$ ratio, suggests closed system differentiation of the magma batch (Figs. 5, 6). However, the Sant'Angelo eruption did not follow the typical pattern of eruptions fed by zoned magma chambers, characterised by withdrawal of progressively less-evolved, deeper magma with time (e.g., Smith and Bailey, 1966; Blake and Ivey, 1986). Instead the eruption was reversely chemically zoned and the more differentiated melt exited the chamber at the end of the eruption. Such zoning has been documented in a number of other volcanic deposits (e.g., Brown et al., 1998; Goff et al., 2013; Takahashi and Nakagawa, 2014) and several reasons have been proposed for it. These include: complex magma reservoir structure involving several isolated reservoirs of variable composition that are ruptured and tapped during an eruption (e.g., Brown et al., 1998; Takahashi and Nakagawa, 2014); non-standard eruption dynamics (e.g., Blake and Ivey 1986); or eruptions supplied from different depths or regions of a magma chamber (Spera and Crisp, 1981). We cannot yet constrain the mechanism to account for the Sant'Angelo zonation. The similarity in isotopic and chemical composition among the last erupted Sant'Angelo magma (phonolite, $^{87}\text{Sr}/^{86}\text{Sr}$ from 0.706557 to 0.706626; CaO=1.02 wt.%; Zr from 1054 to 1080 ppm), the Mago magma (phonolite, $^{87}\text{Sr}/^{86}\text{Sr}$ =0.706537±6; CaO=0.99 wt.%; Zr=1037 ppm) and the first erupted Olummo magma (phonolite, $^{87}\text{Sr}/^{86}\text{Sr}$ from 0.706569 to 0.706519; CaO from 0.97 to 0.92 wt.%; Zr from 1058 to 970 ppm) (Figs. 5, 6), suggests that these eruptions were fed by a compositionally homogeneous reservoir (M1

magma in Figure 9). However, evidence of geochemical zoning is given by the chemistry of the Olummo samples (Figs. 5, 6), which vary from an early extruded differentiated phonolite ($Zr \sim 1100$ ppm; $CaO \sim 1.0$ wt.%) to a late trachyte ($Zr \sim 400$ ppm; $CaO \sim 1.6$ wt.%), indicating a progressive withdrawal of less-differentiated magmas with time. Olummo magmas also show a slightly wider range of $^{87}Sr/^{86}Sr$ ratios (0.70657–0.70642), suggesting replenishment of the pre-Olummo magma chamber by a less radiogenic, less differentiated trachytic magma (M2 magma, Figure 9) that mixed with the trachy-phonolitic resident magma prior to eruption (Fig. 6).

The magma withdrawn during the Tisichiello eruption also exhibits a range of both chemical and isotopic compositions, with a compositional and isotopic gap (Figs. 5, 6, 7). This strengthens arguments for the presence of a chemically and isotopically zoned magma chamber(s). Furthermore, the variation of the Tisichiello magma from trachyte to phonolite during the eruption suggests a complex withdrawal mechanism or magma reservoir arrangement similar to that inferred for the Sant'Angelo eruption. The early erupted Tisichiello magma is isotopically similar to the last erupted Olummo magma, whereas the later, more differentiated Tisichiello magma is more enriched in radiogenic Sr and is separated from the earlier trachyte magma by a Sr isotopic gap (Fig. 6; Table 1). We explain such features as the result of an influx of a more evolved and more radiogenic magma batch raised from the deep reservoir (8–12 km depth) that was more affected by crustal contamination with respect to the other pre-MEGT magmas.

The similarity of $^{87}Sr/^{86}Sr$ among the last erupted Tisichiello, Porticello and MEGT eruptions indicates that they were also fed by the magma of deep provenance more enriched in radiogenic Sr (M3 magma, Figure 9). As the MEGT eruption extruded a large volume of magma (estimates by Brown et al. 2008 and Tomlinson et al. submitted, are in excess of 15 km^3 DRE) and isotopically distinct magma entered the system during the Tisichiello eruption (i.e., several thousand years before), the rate of magma production must have been high. Furthermore, the limited field data suggests that the size of the pre-MEGT eruptions increased through time from the Sant'Angelo to the Tisichiello eruption

The magma that fed the post-caldera collapse La Roia eruption was trachytic, as was the last erupted MEGT melt ($CaO \sim 2.2$ wt.%; $Zr = 290$ ppm), although it was less enriched in radiogenic Sr. The magmas of the Capo Grosso and Chiummano eruptions were less differentiated although isotopically fairly similar to La Roia magma (Fig. 6). It follows that the La Roia, Capo Grosso and Chiummano eruptions

tapped a new and isotopically distinct magma (M4 magma, Figure 9) that rose from the deep reservoir after the MEGT eruption. The later change in composition from trachyte (CaO=1.5 wt.%; Zr=360 ppm) to latite (CaO=4.6 wt.%; Zr=230 ppm) during the Schiappone eruption, coupled with the slightly higher $^{87}\text{Sr}/^{86}\text{Sr}$ ratio (Figs. 5, 6) with respect to La Roia, Capo Grosso and Chiummano magmas, suggests that new, isotopically distinct magma arrived into the shallow system shortly before the Schiappone eruption.

7. Conclusions

Volcanism on Ischia during the time span 75–50 ka BP was affected by variable magma differentiation processes at deep and shallow depths, such as replenishment, fractional crystallization, mixing and assimilation. The Sr and Nd isotopic and geochemical variations through time suggest that the pre-MEGT volcanic activity was characterized by extrusion of magma batches poorly enriched in radiogenic Sr that mostly differentiated at shallow depth, where they attained a $\text{TiO}_2\text{-Fe}_2\text{O}_3$ -rich phonolitic composition through assimilation of a feldspar-rich mush. In particular, during the oldest eruption studied (Sant' Angelo) a quasi-homogeneous magma was extruded (M1 magma, Fig. 9). This magma evolved at shallow depth mainly by fractional crystallization and assimilation. During the Olummo eruption, the magmatic system was recharged by a new, less differentiated and slightly less enriched in radiogenic Sr magma (M2 magma; Fig. 9), that also fed the first phases of the Tisichiello eruption. However, prior to or during the Tisichiello eruption, the magmatic system was recharged by a more enriched in radiogenic Sr magma (M3 magma; Fig. 9), potentially contaminated by both Hercynian crust at 8–12 km depth and by assimilation of feldspar mush at ca. 5 km depth. This magma later fed the climactic MEGT eruption. According to this scenario, the Tisichiello and Porticello events were precursors of the larger MEGT eruption. Volume estimations suggest that at least 15 km^3 of magma accumulated in the shallow feeding system and assimilated residual feldspar cumulates prior to the MEGT eruption. After the MEGT eruption, influx of poorly evolved magma (M4 magma, Fig. 9) resulted in the chemical characteristics of the magmas that fed the later eruptions up to 45 ka BP.

The magmatic history and plumbing system structure explain the variation in magma composition from trachyte to phonolite as a rejuvenation of a sanidine-rich mush by arrival of new trachytic magma. In such a scenario, different P and T conditions are required for the stagnation and differentiation of the pre-

MEGT and MEGT magmas, with respect to the post-MEGT magma. This process could have operated repetitively during the magmatic history of Ischia and could explain the eruption of latitic to phonolitic magmas with a wide range of Sr- and Nd-isotope compositions during the last 10 ka as the result of interaction between magmas and feldspar cumulates.

Acknowledgements

RJB acknowledges a fellowship from the EU Volcano Dynamics Research Training Network (5th Framework Program). The authors thank A. Carandente and P. Belviso for the support in the laboratory. E. Marotta, S. de Vita and F. Sansivero are thanked for help in the field and discussions. This research was partly carried out under the framework of the Italian INGV-DPC 2004–2006 program, sub-project V3-3 Ischia, and PRIN 2008 project. ET, PA and MM were supported by the NERC RESET Consortium (NE/E015905/1). We thank Jon Blundy for editorial stewardship, and Joan Martí and an anonymous reviewer for thoughtful comments on the manuscript.

References

- Appleton JD (1972) Petrogenesis of Potassium-rich lavas from the Roccamonfina Volcano, Roman Region, Italy. *J Petrol* 13:425–456
- Arienzo I, Moretti R, Civetta L, Orsi G, Papale P (2010) The feeding system of Agnano-Monte Spina eruption (Campi Flegrei, Italy): Dragging the past into present activity and future scenarios. *Chem Geol* 270:135–147
- Arienzo I, Heumann A, Wörner G, Civetta L, Orsi G (2011) Processes and timescales of magma evolution prior to the Campanian Ignimbrite eruption (Campi Flegrei, Italy). *Earth Planet Sci Lett* 306:217–228
- Asimow PD, Ghiorso MS (1998) Algorithmic modifications extending MELTS to calculate subsolidus phase relations. *Am Mineral* 83:1127–1132
- Auger E, Gasparini P, Virieux J, Zollo A (2001) Seismic evidence of an extended magmatic sill under Mt. Vesuvius. *Science* 294:1510–1512 DOI: 10.1126/science.1064893
- Bachmann O, Bergantz GW (2008) The Magma Reservoirs that Feed Super-eruptions. *Elements* 4:17–21
- Bacon CR, Druitt TH (1988) Compositional evolution of the zoned calcalkaline magma chamber of Mount Mazama, Crater Lake, Oregon. *Contrib Mineral Petrol* 98:224–256 doi: 10.1007/bf00402114
- Blake S, Ivey GN (1986) Density and viscosity gradients in zoned magma chambers, and their influence on withdrawal dynamics. *J Volcanol Geotherm Res* 30:201–230
- Blake S, Ivey GN (1986) Magma-mixing and the dynamics of withdrawal from stratified reservoirs. *J Volcanol Geotherm Res* 27: 153–178
- Brown RJ, Orsi G, de Vita S (2008) New insights into Late Pleistocene explosive volcanic activity and caldera formation on Ischia (southern Italy). *Bull Volcanol* 70:583–603
- Brown SJA, Wilson CJN, Cole JW, Wooden J (1998) The Whakamaru group ignimbrites, Taupo Volcanic Zone, New Zealand: evidence for reverse tapping of a zoned silicic magmatic system. *J Volcanol Geotherm Res* 84:1–37
- Bruno P, de Alteriis G, Florio G (2002) The western undersea section of the Ischia volcanic complex (Italy, Tyrrhenian Sea) inferred by marine geophysical data. *Geophys Res Lett* 23:2689–2692

Buchner G, Italiano A, Vita-Finzi C (1996) Recent uplift of Ischia, Southern Italy. In: McGuire WJ, Jones AP, Neuberg J (Eds) *Volcano instability on the Earth and other planets*. Geol Soc London Spec Pub 110:249–252

Burgisser A, Bergantz GW (2011) A rapid mechanism to remobilize and homogenize highly crystalline magma bodies. *Nature* 471:212–U97, DOI: 10.1038/nature09799

Caliro S, Panichi C, Stanzione D (1999) Variation in the TDC isotope composition of thermal waters of the island of Ischia (Italy) and its implications for volcanic surveillance. *J Volcanol Geotherm Res* 90:219–240

Cannatelli C, Lima A, Bodnar RJ, De Vivo B, Webster JD, Fedele L (2007) Geochemistry of melt inclusions from the Fondo Riccio and Minopoli 1 eruptions at Campi Flegrei (Italy). *Chem Geol* 237:418–432, DOI: 10.1016/j.chemgeo.2006.07.012

Cashman, KV Sparks, RSJ (2013) How volcanoes work: A 25 year perspective. *Geol Soc Am Bull* 125:664–690 DOI: 10.1130/B30720.1

Charlier BLA, Wilson CJN, Davidson JP (2008) Rapid open-system assembly of a large silicic magma body: time-resolved evidence from cored plagioclase crystals in the Oruanui eruption deposits, New Zealand. *Contrib Mineral Petrol* 156:799–813, DOI: 10.1007/s00410-008-0316-y

Charlier BLA, Wilson CJN (2010) Chronology and Evolution of Caldera-forming and Post-caldera Magma Systems at Okataina Volcano, New Zealand from Zircon U-Th Model-age Spectra. *J Petrol* 51:1121–1141, DOI: 10.1093/petrology/egq015

Cioni R, Marianelli P, Santacroce R (1998) Thermal and compositional evolution of the shallow magma chambers of Vesuvius: Evidence from pyroxene phenocrysts and melt inclusions. *J. Geophys. Res.* 103: doi: 10.1029/98JB01124. issn: 0148-0227

Civetta L, Gallo G, Orsi G (1991) Sr- and Nd-isotope and trace element constraints on the chemical evolution of Ischia (Italy) in the last 55 ka. *J Volcanol Geotherm Res* 46:213-230

Crisci GM, de Francesco AM, Mazzuoli R, Poli G, Stanzione D (1989) Geochemistry of the recent volcanics of Ischia Island, Italy: evidences of crystallization and magma mixing. *Chem Geol* 78:15–33

Czamanske GK and Wones DR (1973) Oxidation during magmatic differentiation, Finnmarka Complex, Oslo area, Norway: Part 2: The mafic silicates. *J Petrol* 14:349–380

D'Antonio M (2011) Lithology of the basement underlying the Campi Flegrei caldera: volcanological and petrological constraints. *J Volcanol Geotherm Res* 200:91–98, doi:10.1016/j.jvolgeores.2010.12.006

D'Antonio M, Tonarini S, Arienzo I, Civetta L, Di Renzo V (2007) Components and processes in the magma genesis of the Phlegrean Volcanic District, southern Italy. In Beccaluva L, Bianchini G and Wilson M (Eds) “Cenozoic Volcanism in the Mediterranean Area”. *Geol Soc Am Spec Pap* 418:203–220, doi:10.1130/2007.2418(10)

D'Antonio M, Tonarini S, Arienzo I, Civetta L, Dallai L, Moretti R, Orsi G, Andria M, Trecalli A (2013) Mantle and crustal processes in the magmatism of the Campania region: inferences from mineralogy, geochemistry, and Sr-Nd-O isotopes of young hybrid volcanics of the Ischia island (South Italy). *Contrib Mineral Petrol* 165:1173–1194, doi:10.1007/s00410-013-0853-x

de Vita S, Sansivero F, Orsi G, Marotta E (2006) Cyclical slope instability and volcanism related to volcano-tectonism in resurgent calderas: the Ischia island (Italy) case study. *Eng Geol* 86:148–165, doi:10.1016/j.enggeo.2006.02.013

de Vita S, Sansivero F, Orsi G, Marotta E, Piochi M (2010) Volcanological and structural evolution of the Ischia resurgent caldera (Italy) over the past 10 ka. In Groppelli G and Viereck-Goette L (Eds) "Stratigraphy and Geology of Volcanic Areas". Geol Soc Am Spec Pap 464:193–241, doi:10.1130/2010.2464(10)

Della Seta M, Marotta E, Orsi G, de Vita S, Sansivero F, Fredi P (2012) Slope instability induced by volcano-tectonism as an additional source of hazard in active volcanic areas: the case of Ischia island (Italy). Bull Volcanol 74:79–106, doi:10.1007/s00445-011-0501-0

Di Girolamo P, Ghiara MR, Rolandi G, Stanzione D (1979). Caratteri geochemici delle vulcaniti quaternarie della Campania (calc-alcaline, shoshonitiche, leucitiche): osservazioni geotettoniche e genetiche. Rend SIMP 35:361-375

Di Girolamo P, Melluso L, Morra V, Secchi FAG (1995) Evidence of interaction between mafic and differentiated magmas in the youngest phase of activity at Ischia Island (Italy). Per Mineral 64:393–411

Di Napoli R, Aiuppa A, Bellomo S, Brusca L, D'Alessandro W, Gagliano Candela E, Longo M, Pecoraino G, Valenza M (2009) A model for Ischia hydrothermal system: Evidences from the chemistry of thermal groundwaters. J Volcanol Geotherm Res 186:133–159, doi:10.1016/j.jvolgeores.2009.06.005

Di Napoli R, Federico C, Aiuppa A, D'Antonio M, Valenza M (2013) Quantitative models of hydrothermal fluid-mineral reaction: The Ischia case. Geochim Cosmochim Acta 105:108–129, doi:10.1016/j.gca.2012.11.039

Di Napoli R, Martorana R, Orsi G, Aiuppa A, Camarda M, De Gregorio S, Gagliano Candela E, Luzio D, Messina N, Pecoraino G, Bitetto M, de Vita S, Valenza M (2011) Highlights on the structure of hydrothermal systems from an integrated geochemical, geophysical and geological approach: the Ischia Island case study. Geochim Geophys Geosys 12, Q07017, doi:10.1029/2010GC003476

Di Renzo V, Arienzo I, Civetta L, D'Antonio M, Tonarini S, Di Vito MA, Orsi G (2011) The magmatic feeding system of the Campi Flegrei caldera: Architecture and temporal evolution. Chem Geol 281:227–241

Druitt TH, Costa F, Deloule E, Dungan M, Scaillet B (2012) Decadal to monthly timescales of magma transfer and reservoir growth at a caldera volcano. Nature 482:77–U97, DOI: 10.1038/nature10706

Fabbrizio A, Scaillet B, Carroll MR (2009) Estimation of pre-eruptive magmatic water fugacity in the Phlegrean Fields, Naples, Italy. Eur J Mineral 21:107–116

Foden, J (1986) The petrology of Tambora volcano, Indonesia - a model for the 1815 eruption. J Volcanol Geotherm Res 27:1–41 DOI: 10.1016/0377-0273(86)90079-X

Forcella F, Gnaccolini M, Vezzoli L (1981) Stratigrafia e sedimentologia dei depositi piroclastici affioranti nel settore sud-occidentale dell'isola d'Ischia. Riv It Paleont Strat 87:329–366

Forcella F, Gnaccolini M, Vezzoli L (1982) I depositi piroclastici del settore sud-orientale dell'isola d'Ischia (Italia). Riv It Paleont Strat 89:135–170

Ghiara MR, Lirer L, Munno R (1979) Mineralogy and geochemistry of the "low-potassium series" of the Campania volcanics (South Italy). Chem Geol 26:29–49

Ghiorso MS, Sack RO (1995) Chemical mass-transfer in magmatic processes. A revised and internally consistent thermodynamic model for the interpolation of liquid-solid equilibria in magmatic systems at elevated temperatures and pressures. Contrib Mineral Petrol 119:197–212

- Gillot PY, Chiesa S, Pasquaré G, Vezzoli L (1982) < 33 000 yr K/Ar dating of the volcano-tectonic horst of the isle of Ischia, Gulf of Naples. *Nature* 229:242
- Ginibre C, Wörner G (2007) Variable parent magmas and recharge regimes of the Parinacota magma system (N. Chile) revealed by Fe, Mg and Sr zoning in plagioclase. *Lithos* 98: 118-140
- Goff F, Warren RG, Goff CJ, Dunbar N (2014) Eruption of reverse-zoned upper Tshirege Member, Banderlier Tuff from centralized vents within Valles Caldera, New Mexico. *J Volcanol Geotherm Res* 276: 82-104
- Goldstein SL, Deines P, Oelkers EH, Rudnick RL, Walter LM (2003) Standards for publications of isotope ratio and chemical data in *Chemical Geology*. *Chem Geol* 202:1-4
- Gunow AJ, Ludington S, and Munoz JL (1980) Fluorine in micas from the Henderson molybdenite deposit, Colorado. *Econ Geol* 75:1127-1137
- Inguaggiato S, Pecoraino G, D'Amore F (2000) Chemical and isotopic characterization of fluid manifestations of Ischia Island (Italy). *J Volcanol Geotherm Res* 99:151-178
- Le Maitre RW, Bateman P, Dudek A, Keller J, Lameyr J, Le Bas MJ, Sabine PJ, Schmid R, Sørensen H, Streckeisen A, Woolley AR, Zanettin B (eds) (1989) *A Classification of Igneous Rocks and Glossary of Terms: Recommendations of the International Union of Geological Sciences, Subcommittee on the Systematics of Igneous Rocks*. Oxford: Blackwell Scientific, pp 193
- Mangiacapra A, Moretti R, Rutherford M, Civetta L, Orsi G, Papale P (2008) The deep magmatic system of the Campi Flegrei caldera (Italy). *Geophys Res Lett* 35 doi: 10.1029/2008GL035550
- Moretti R, Arienzo I, Orsi G, Civetta L, D'Antonio M (2013) The deep plumbing system of Ischia: a physico-chemical window on the fluid-saturated and CO₂-sustained Neapolitan volcanism (Southern Italy). *J Petrol* 54:951-984, doi:10.1093/petrology/egt002
- Munoz, JL (1984) F-OH and Cl-OH exchange in micas with applications to hydrothermal ore deposits. *Miner Soc Am Rev Min* 13:469-494
- Orsi G, Gallo G, Zanchi A (1991) Simple-shearing block resurgence in caldera depressions. A model from Pantelleria and Ischia. *J Volcanol Geotherm Res* 47:1-11
- Orsi G, Patella D, Piochi M, Tramacere A (1999) Magnetic modelling of the Phlegraean Volcanic District with extension to the Ponza archipelago, Italy. *J Volcanol Geotherm Res* 91:345-360
- Orsi G, Piochi M, Campajola L, D'Onofrio A, Gialanella L, Terrasi F (1996) ¹⁴C geochronological constraints for the volcanic history of the island of Ischia (Italy) over the last 5000 years. *J Volcanol Geotherm Res* 71:249-257
- Pabst S, Wörner G, Civetta L, Tesoro R (2008) Magma chamber evolution prior to the Campanian Ignimbrite and Neapolitan Yellow Tuff eruptions (Campi Flegrei, Italy). *Bull Volcanol* 70:961-976, doi:10.1007/s00445-007-0180-z
- Paoletti V, D'Antonio M, Rapolla A (2013) The structural setting of the Ischia Island (Phlegraean Volcanic District, Southern Italy): Inferences from geophysics and geochemistry. *J Volcanol Geotherm Res* 249:155-173

- Paoletti V, Di Maio R, Cella F, Florio G, Mocka K, Roberti N, Secomandi M, Supper R, Fedi M, Rapolla A (2009) The Ischia volcanic island (Southern Italy): inferences from potential field data interpretation. *J Volcanol Geotherm Res* 179:69–86
- Papale P, Moretti R, Barbato D (2006) The compositional dependence of the saturation surface of H₂O+CO₂ fluids in silicate melts. *Chem Geol* 229:78–95
- Piochi M, Civetta L, Orsi G (1999) Mingling in the magmatic system of Ischia (Italy) in the past 5 ka. *Mineral Petrol* 66:227–258
- Poli S, Chiesa S, Gillot P–Y, Gregnanin A, Guichard F (1987) Chemistry versus time in the volcanic complex of Ischia (Gulf of Naples, Italy): evidence of successive magmatic cycles. *Contrib Mineral Petrol* 95:322–335
- Poli S, Chiesa S, Gillot P–Y, Guichard F, Vezzoli L (1989) Time dimension in the geochemical approach and hazard estimates of a volcanic area: the isle of Ischia. *J Volcanol Geotherm Res* 36:327–335
- Rapolla A, Paoletti V, Secomandi M (2010) Seismically-induced landslide susceptibility evaluation: application of a new procedure to the island of Ischia, Campania Region, Southern Italy. *Engin Geol* 114:10–25
- Righter K, Carmichael ISE (1996) Phase equilibria of phlogopite lamprophyres from western Mexico: biotite-liquid equilibria and P-T estimates for biotite-bearing igneous rocks. *Contrib Mineral Petrol* 123:1–21
- Rittmann A, Gottini V (1981) L'isola d'Ischia - Geologia. *Boll Serv Geol Italia* 101:131–274
- Rosi M, Sbrana A, Vezzoli L (1988) Correlazioni tefrostratigrafiche di alcuni livelli di Ischia, Procida e Campi Flegrei. *Mem Soc Geol It* 41:1015–1027
- Rottura A, Del Moro A, Pinarelli L, Petrini R, Peccerillo A, Caggianelli A, Bargossi GM, Piccarreta G (1991) Relationships between intermediate and acidic rocks in orogenic granitoid suites: petrological, geochemical and isotopic (Sr, Nd, Pb) data from Capo Vaticano (southern Calabria, Italy). *Chem Geol* 92:153–176
- Sbrana A, Fulignati P, Marianelli P, Boyce AJ, Cecchetti A (2009) Exhumation of an active magmatic–hydrothermal system in a resurgent caldera environment: the example of Ischia (Italy). *J Geol Soc Lond* 166:1061–1073
- Smith RL, Bailey RA (1966) The Bandelier Tuff: a study of ash-flow eruption cycles from zoned magma chambers. *Bull Volcanol* 29:83–103
- Smith PM, Asimow, PD (2005) *Adiabat_1ph*: A new public front-end to the MELTS, pMELTS, and pHMELTS models Author(s): Smith, PM; Asimow, PD, *Geochem Geophys Geosys* 6, Q02004 DOI: 10.1029/2004GC000816
- Spera FJ, Crisp JA (1981) Eruption volume, periodicity, and caldera area: relationships and inferences on development of compositional zonation: I silicic chambers. *J Volcanol Geotherm Res* 11:169–187
- Spera FJ, Bohrsen WA (2001) Energy-constrained open-system magmatic processes I: general model and energy-constrained assimilation and fractional crystallization (EC-AFC) formulation. *J Petrol* 42:999–1018
- Storner JC, Nicholls JA (1978) XLFAC: A program for interactive testing of magmatic differentiation models. *Comp Geosci* 4:143–159

- Takahashi R, Nakagawa M (2013) Formation of a compositionally reverse zoned magma chamber: petrology of the AD1694 eruptions of Hokkaido-Komagatake volcano, Japan. *J Petrol* 54:815-838
- Tibaldi A, Vezzoli L (1998) The space problem of caldera resurgence: an example from Ischia Island, Italy. *Geolog Rundt* 87:53–66
- Tibaldi A, Vezzoli L (2004) A new type of volcano flank failure: the resurgent caldera sector collapse, Ischia, Italy. *Geophys Res Lett* 31:L14605, doi: 10.1029/2004GL020419
- Tomlinson EL, Albert PG, Wulf S, Brown RJ, Smith VC, Keller J, Orsi G, Bourne AJ, Menzies MA (accepted) Age and geochemistry of tephra layers from Ischia, 1 Italy: constraints from proximal distal correlations with Lago Grande di Monticchio. *J Volcanol Geotherm Res*
- Tonarini S, Leeman WP, Civetta L, D'Antonio M, Ferrara G, Necco A (2004) B/Nb and $\delta^{11}\text{B}$ systematics in the Phlegrean Volcanic District (PVD). *J Volcanol Geotherm Res* 133:123–139
- Vezzoli L (Ed) (1988) Island of Ischia. *Quaderni de La Ricerca Scientifica, CNR, Rome* 114: pp 133
- Waldbaum DR and Thompson JB (1969) Mixing properties of sanidine crystalline solutions IV: Phase diagrams from equations of state. *Am Mineral* 54:1274–1298
- Wiesmaier S, Deegan FM, Troll VR, Carrecedo JC, Chadwick JP, Chew DM (2012) Magma mixing in the 1100 AD Montaña Reventada composite lava flow, Tenerife, Canary Islands: interaction between rift zone and central volcano plumbing systems. *Contrib Mineral Petrol* 162:651–669
- Wones DR, Eugster HP (1965) Stability of biotite: experiment, theory and application. *Am Mineral* 50:1228–1272
- Woodland AB, Wood, BJ (1994) Fe_3O_4 activities in Fe-Ti spinel solid solutions. *Eur J Mineral* 6:23–37
- Zollo, A, Maercklin N, Vassallo M, Dello Iacono D, Virieux J, Gasparini P (2008) Seismic reflections reveal a massive melt layer feeding Campi Flegrei caldera. *Geophys Res Lett* 35:L12306 DOI: 10.1029/2008GL034242

Figure Captions

Figure 1. Geological map of Ischia showing the outcrop of rocks of different ages on the island.

Figure 2. Summary volcanic stratigraphy for the period ~75–55 ka on Ischia (modified from Brown et al. 2008).

Figure 3. Locations of samples within the different volcanic rock units on Ischia. Stratigraphic logs modified from Brown et al. (2008). Thicknesses in metres (note variable scale).

Figure 4. Total alkali-silica plot for the volcanic rocks erupted in the study period, on Ischia. Grey shaded area represents all analyses from Ischia. Data from Vezzoli (1988), Crisci et al. (1989) and Civetta et al. (1991)

Figure 5. Harker diagrams. 5a) CaO vs. major elements contents; 5b) CaO vs. selected trace elements contents. Red symbols refer to products older than MEGT (pre-MEGT), green symbols to the MEGT and blue symbols to products younger than the MEGT eruption (post-MEGT). Fields are built one data relative to glasses from the same samples (Tomlinson et al., submitted).

Figure 6. Chemostratigraphy. Red symbols refer to products older than MEGT (pre-MEGT), green symbols to the MEGT and blue symbols to products younger than the MEGT eruption (post-MEGT). Fields are built on data relative to glasses from the same samples (Tomlinson et al., submitted).

Figure 7. $^{87}\text{Sr}/^{86}\text{Sr}$ vs $^{143}\text{Nd}/^{144}\text{Nd}$ isotope compositions relative to the investigated products. In the main plot isotope ratios are plotted together with results from EC-AFC modelling (blue line). In the insert the 75–50 ka erupted products are compared with the fields built on the isotope compositions of Procida, Ischia Campi Flegrei erupted products, from literature.

Figure 8. Results of least-squared mass balance calculations (Stormer and Nicholls, 1978) have been plotted as purple circles. The first step (blue line) as been modelled from the composition of the poorly evolved (latite) Chiummano sample (OIS 0324) in order to get a trachytic daughter magma similar to the first-erupted Schiappone magma (MEGT 0312) (Table 3). From the latter magma, a second step of fractional crystallization (green line) allow us to partially explain the composition of the residual glasses. Conversely, if using the MELTS code, feldspar assimilation and fractional crystallization are required for reproducing, starting from a magma compositionally similar to the MEGT 0308, the chemical composition of the evolved trachyte magma represented by sample MEGT 0312 (Step 2 in Table 4).

Figure 9. Cartoon illustrating the sequence of arrival of different magma batches (M1-M4) into the deep and shallow magmatic plumbing system beneath Ischia for the studied period. Time and depth are not to scale.

Appendix

A1. Fluid-mineral equilibria

Following Fabbrizio et al. (2009), activity values for sanidine were taken by graphically reading the activity-composition plot in Waldbaum and Thompson (1989), those for magnetite by using the activity-composition expression of Woodland and Wood (1994) along the join magnetite-ulvospinel, and those for annite by the ionic model of Czamanske and Wones (1973). Calculations at 930°C return f_{H_2O} values of 668 bars and 498 bars for the least (NNO+0.75) and most oxidized (NNO+1.44) trachyte (or trachy/phonolites), respectively. Furthermore, we computed the f_{HF} and f_{HCl} by using the expressions for chemical exchanges between fluoroannite/phlogopite – annite/fluorophlogopite and chloroannite/phlogopite – annite/chlorophlogopite pairs from Munoz (1984), based on the compositional deconvolution of Gunow et al. (1980) for the siderophyllite and annite components in biotites. We obtained $f_{HF}=0.4$ bars and $f_{HCl}=335$ bars at NNO+0.75, and $f_{HF} < 0.1$ bars and $f_{HCl}=18$ bars at NNO+1.44.

A2. MELTS calculations

For the parental latite ascending from depth larger than 6 km, we lack a direct temperature-estimate as well as information on volatile contents. By analogy with younger than 3 ka Ischia latites (Moretti et al. 2013), temperatures around 1200°C and maximum water contents of 3-3.5 wt% can be suggested for the Chiummano latite. Of note is that the application of the CaO-in-glass thermometer of Cioni et al. (1998) returns a temperature of 1060°C.

MELTS calculations were thus initialized with a starting composition represented by the Chiummano latite (Table 1, 4) having 2.5 wt% of water, f_{O_2} conditions of QFM+1 (i.e., NNO+~ 0.6), the latter more reduced than biotites in poorly evolved trachytes, and initial P and T at 200 MPa and 1200°C, respectively. The crystallizing solid phases are those consistent with petrographic description (see also Table 4). A $\Delta P/\Delta T$ gradient of 2.6 bar/°C was applied in such a way that 930°C were reached at 130 MPa (5.5 km). In this P-T conditions the poorly evolved trachyte magma forms. After crystallization of clinopyroxene, Ti-magnetite, plagioclase, minor olivine and biotite, the residual liquid (72%) attains a composition close to MEGT 0308 trachyte sample (Step 1 in Table 4). Interestingly, biotite starts crystallizing between 940 and 930°C for the selected water content. An initial water content larger than 2.5 wt% would prevent crystallization of biotite.

The following step requires assimilation of felsic rocks to approach the composition of the MEGT 0312 sample, otherwise, fractional crystallization would only drive the system towards more silica-undersaturated compositions. The assimilant was composed by two feldspars (Na-sanidine and K-sanidine) whereas the assimilating magma was represented by the trachyte, derived by fractional crystallization from the parental latite at 930°C. Table 4 in text reports the MELTS outcomes for the assimilation process, in which feldspars, initially at 600°C, are isobarically and isothermally assimilated by the trachyte at 930°C. Incremental assimilation of P₂O₅- and TiO₂-free feldspars give results that are in line with the Schiappone trachy-phonolitic MEGT 0312 composition (Step 2 in Table 4 and figure 8), allowing a slight decrease of P₂O₅ and TiO₂ content (this latter favored by concomitant precipitation of Ti-magnetite).

Alternatively, feldspar assimilation can involve directly the latite (1200°C), ascending between 130 and 100 MPa and infiltrating feldspar cumulitic residuals. If this is the case, during feldspar digestion water is lost, and dissolved H₂O falls down to 1 wt% in the final melt. In the absence of a detailed melt inclusion study, we will retain here the first scenario, involving feldspar assimilation from trachyte at 930°C. It is also worth noting that during assimilation, fractionated solids, which amount are nearly equal in mass to that of assimilated feldspars, are dominated by feldspar Or₆₀₋₆₇. This implies that, after each assimilation event, feldspar cumulates are potentially left in place for future remobilization.

After feldspar assimilation fractional crystallization drives again the residual liquid towards undersaturation, with SiO₂ reaching 55-56 wt% and Al₂O₃ dropping inevitably, accompanied by a significant decrease of FeO_{tot} and TiO₂. Only a depressurization taking place right after assimilation allows to keep high silica and alumina contents, nearly constant FeO_{tot} and to increase TiO₂, consistent with observations (step 3 in table 4).

After assimilation, and during this final stage of isothermal decompression, biotite, two feldspars, spinel and apatite crystallise. This association is observed only by keeping QFM+2. Lower oxygen fugacities promote olivine, whereas higher values do not allow Na₂O to overcome K₂O. Nepheline crystallizes at the very end (T=910°C and P=100 bar; see MELTS step 4 in Table 4), when the residual liquid amounts to 3.5 wt%. However, liquid composition at that stage would be even more evolved than that in step 3 (Table 4).

Finally, we remark that MELTS cannot be used to investigate accessory phases such as sphene, apatite and Na-amphiboles, at least for the studied compositions, for which the role of fluids other than water (S-species, halogens) may have dramatic effects on the mixing properties of such solid solutions.

	SiO ₂	TiO ₂	Al ₂ O ₃	Fe ₂ O ₃	MnO	MgO	CaO	Na ₂ O	K ₂ O	P ₂ O ₅	LO1	A.I.
Schiappone												
MEGT 0315	60.37	0.44	18.46	3.21	0.14	1.10	2.10	5.41	7.48	0.13	non dosè	0.92
MEGT 0317	60.71	0.40	18.46	2.91	0.11	0.77	1.76	4.78	8.08	0.09	non dosè	0.90
MEGT 0316	61.99	0.39	18.59	2.79	0.13	0.53	1.49	5.54	8.09	0.09	non dosè	0.96
MEGT 0311	60.31	0.46	18.24	3.27	0.14	1.47	2.40	4.84	7.38	0.14	non dosè	0.87
MEGT 0310	60.04	0.48	18.49	3.48	0.13	1.59	2.73	5.25	7.46	0.18	non dosè	0.90
MEGT 0309	56.46	0.59	17.63	4.65	0.13	3.27	4.52	4.33	6.39	0.29	non dosè	0.80
MEGT 0308	60.19	0.46	18.32	3.19	0.13	1.20	2.27	5.27	7.43	0.13	non dosè	0.91
MEGT 0307	60.51	0.46	18.43	3.26	0.14	1.23	2.42	5.43	7.42	0.16	non dosè	0.92
MEGT 0306	59.07	0.45	18.00	3.31	0.12	1.20	2.39	5.26	7.28	0.14	2.57	0.92
MEGT 0314	61.72	0.42	18.70	2.72	0.14	0.63	1.56	5.71	7.50	0.10	non dosè	0.94
MEGT 0313	60.40	0.39	18.12	2.65	0.13	0.59	1.40	5.36	7.32	0.08	3.34	0.92
MEGT 0312	61.49	0.41	18.57	2.68	0.14	0.56	1.50	5.46	7.51	0.10	non dosè	0.92
MEGT 0305	58.39	0.54	18.08	4.07	0.14	2.03	3.64	4.83	6.90	0.23	non dosè	0.85
Chiummano												
OIS 0324	54.52	0.78	16.77	6.27	0.13	4.45	6.97	3.37	5.46	0.35	1.04	0.68
Capo grosso												
OIS 0323	58.44	0.50	18.21	3.66	0.12	1.05	2.58	4.61	7.35	0.22	3.10	0.85
La Roya												
OIS 0322	60.85	0.48	18.83	3.44	0.13	0.95	2.18	5.52	7.25	0.18	non dosè	0.90
Upper Monte Epomeo												
MEGT 0318	58.42	0.37	17.77	2.67	0.10	1.08	2.61	5.41	3.82	0.11	7.48	0.73
MEGT 0319	41.09	0.50	13.23	3.83	0.50	2.91	15.57	2.60	5.97	0.20	13.46	0.81
MEGT 0328	56.81	0.40	17.08	2.75	0.11	0.96	2.40	5.15	3.43	0.09	10.65	0.71
Lower Monte Epomeo												
MEGT 0301	62.19	0.46	18.55	2.65	0.10	0.36	1.18	5.44	7.90	0.08	0.87	0.94
OIS 0319	61.35	0.47	18.55	2.84	0.16	0.62	1.47	6.05	7.24	0.11	non dosè	0.96
OIS 0337	60.77	0.56	18.03	3.20	0.21	0.50	1.44	7.30	6.32	0.08	1.10	1.05
OIS 0338	60.74	0.57	17.97	3.24	0.22	0.52	1.44	7.29	6.29	0.08	1.50	1.05
OIS 0339	60.51	0.50	17.76	2.74	0.17	0.38	1.22	6.59	6.64	0.07	2.96	1.01
OIS 0340	59.81	0.53	17.74	2.89	0.23	0.31	1.06	7.44	6.17	0.05	2.80	1.07
OIS 0325	60.97	0.53	18.54	3.04	0.26	0.45	1.02	7.53	6.35	0.06	1.10	1.04
OIS 0333	61.73	0.51	18.68	3.10	0.25	0.60	0.98	7.32	6.58	0.10	non dosè	1.03
OIS 0321	61.34	0.51	18.55	3.07	0.28	0.43	1.00	7.70	6.47	0.12	non dosè	1.06
Porticello												
OIS 0320	60.75	0.53	18.64	2.91	0.24	0.47	1.08	6.95	6.51	0.11	non dosè	0.99
OIS 0316	60.74	0.53	18.38	2.91	0.24	0.50	1.08	7.16	6.46	0.11	non dosè	1.02
Tisichiello 60ka												
OIS 0315	60.23	0.50	18.46	3.11	0.23	0.57	1.27	7.04	6.65	0.15	non dosè	1.02
OIS 0314	58.67	0.47	18.22	2.95	0.29	0.39	1.04	7.76	6.36	0.11	3.59	1.08
OIS 0313	58.61	0.47	18.03	2.90	0.26	0.49	1.09	7.68	6.40	0.09	3.82	1.08
OIS 0312	59.40	0.48	18.02	2.94	0.16	0.64	1.37	5.90	6.98	0.12	3.79	0.96
OIS 0311	60.20	0.49	18.30	3.06	0.16	0.66	1.43	6.09	7.15	0.11	2.27	0.97
OIS 0310	58.94	0.50	18.01	3.24	0.14	0.84	1.75	5.68	7.11	0.15	3.46	0.95
OIS 0309	59.44	0.47	18.17	2.91	0.16	0.59	1.37	6.06	7.17	0.12	3.35	0.98
OIS 0308	58.79	0.49	18.12	3.04	0.15	0.68	1.62	5.88	6.85	0.14	non dosè	0.94
Olummo 65												
OIS 0318	60.37	0.50	18.51	3.17	0.16	0.65	1.53	6.32	7.36	0.15	1.08	0.99
OIS 0317	61.20	0.54	18.79	3.38	0.16	0.89	1.74	6.01	6.83	0.18	non dosè	0.92
OIS 0307	59.48	0.49	18.28	3.01	0.16	0.60	1.40	6.20	6.90	0.14	non dosè	0.97
OIS 0306	58.53	0.53	18.11	3.08	0.21	0.63	1.19	6.53	6.69	0.12	non dosè	0.99
OIS 0305	58.25	0.56	17.81	3.19	0.29	0.54	1.01	7.67	6.32	0.10	4.11	1.09
OIS 0304	58.59	0.53	17.81	3.06	0.31	0.49	0.92	7.90	6.27	0.06	3.92	1.11
OIS 0303	58.36	0.52	17.75	3.10	0.30	0.51	0.92	7.77	6.44	< L.D.	4.18	1.11
OIS 0302	58.21	0.52	17.93	3.10	0.30	0.68	0.97	7.87	6.28	0.11	non dosè	1.10
Mago 68												
OIS 0301	58.09	0.53	17.68	3.11	0.30	0.99	0.99	7.41	5.94	0.05	non dosè	1.05
Sant'angelo 70												
OIS 0332	60.66	0.56	18.74	3.31	0.32	0.49	1.02	8.13	6.41	0.11	non dosè	1.08
OIS 0331	61.05	0.56	18.87	3.26	0.31	0.41	1.02	8.32	6.08	0.09	non dosè	1.07
OIS 0330	61.18	0.50	18.61	2.96	0.26	0.34	1.10	7.70	6.62	0.13	non dosè	1.07
OIS 0329	60.08	0.55	18.60	3.24	0.20	0.71	1.52	6.49	7.00	0.14	non dosè	0.98
OIS 0328	60.17	0.56	18.33	3.03	0.23	0.50	1.15	6.80	6.78	0.11	2.25	1.01
OIS 0327	60.43	0.55	18.42	3.02	0.22	0.54	1.25	7.23	6.82	0.12	1.25	1.05
OIS 0326	61.20	0.57	18.69	3.06	0.24	0.55	1.13	7.23	6.92	0.12	non dosè	1.04
Barano												
OIS 0334	60.92	0.50	18.54	3.25	0.16	0.70	1.51	5.64	7.54	0.12	0.91	0.94

* Age corrected isotope ratios

Different aliquot of feldspar crystals

Table 1. Major, trace and isotope data for the studied rocks.

	Be	V	Cr	Co	Ni	Cu	Zn	Ga	Ge	As	Rb	Sr	Y	Zr	Nb	Mo	Sn	Sb	Cs	Ba	La	Ce	
Schiappone																							
MEGT 0315	7.4	47.6	14.4	3.8	7.2	6.0	63.9	18.4	1.4	7.0	262.7	109.5	34.0	306.4	40.3	3.9	3.7	0.42	11.4	131.0	69.1	133.4	
MEGT 0317	5.2	37.2 < L.D.		2.0 < L.D.	< L.D.		56.3	16.5	1.3	5.6	229.6	79.1	26.2	228.2	30.8	3.0	3.0	0.41	8.6	61.3	56.1	107.6	
MEGT 0316	6.4	36.4 < L.D.		1.8 < L.D.	< L.D.		62.3	18.3	1.4	6.6	263.5	47.6	31.6	283.3	37.3	3.5	3.6	0.36	10.4	31.9	66.0	125.3	
MEGT 0311	7.6	46.9	25.4	4.7	9.7	8.9	60.9	18.1	1.5	7.1	249.9	125.5	31.9	310.8	40.4	3.5	3.8	0.50	10.8	157.1	69.9	134.2	
MEGT 0310	7.6	57.7	25.4	5.5	12.4	10.8	64.8	18.3	1.5	7.1	257.6	161.1	34.6	300.6	39.4	3.8	3.8	0.42	11.1	208.1	71.3	133.1	
MEGT 0309	5.7	96.6	64.1	12.3	31.4	20.8	61.4	16.9	1.5	5.6	208.9	364.2	28.5	227.3	30.3	3.1	3.1	0.31	8.6	501.3	59.2	107.3	
MEGT 0308	7.4	50.3	15.0	3.9	6.2	9.4	64.9	18.3	1.5	7.2	261.8	125.1	33.6	306.0	39.9	4.0	3.8	0.41	11.3	161.5	70.7	132.4	
MEGT 0307	7.5	53.1	21.8	4.4	7.5	10.8	66.1	18.9	1.5	7.2	263.6	125.2	34.4	323.7	40.4	3.9	3.9	0.41	11.5	159.2	71.2	134.1	
MEGT 0306	7.2	56.4	25.1	5.1	11.3	9.4	64.1	19.1	1.5	7.0	269.0	146.8	34.4	306.1	41.0	4.2	3.7	0.42	11.3	186.2	71.9	133.5	
MEGT 0314	7.9	32.6 < L.D.		1.7 < L.D.		3.8	70.3	19.7	1.5	8.1	283.5	30.6	36.8	359.3	45.5	4.6	4.1	0.47	12.8	22.9	75.4	146.7	
MEGT 0313	8.2	33.6	6.4	1.6 < L.D.		3.3	70.8	20.1	1.7	8.1	283.7	30.6	36.1	364.9	45.8	4.5	4.2	0.48	12.7	21.9	75.9	146.8	
MEGT 0312	8.2	32.1 < L.D.		1.5 < L.D.		4.2	69.2	19.4	1.5	8.2	282.0	28.7	36.5	358.6	45.0	4.4	4.1	0.51	12.6	20.4	74.3	143.8	
MEGT 0305	6.3	76.6	39.0	8.2	16.4	15.2	64.9	17.7	1.4	6.1	245.1	262.6	31.4	271.0	35.9	3.6	3.5	0.35	10.2	373.3	65.5	123.5	
Chiummano																							
OIS 0324	3.8	144.3	174.3	18.8	45.2	16.7	64.6	15.8	1.4	2.8	151.9	547.6	23.0	128.4	19.3	1.8	3.0	0.30	5.0	595.0	36.3	75.6	
Capo grosso																							
OIS 0323	4.6	57.5	9.1	4.1	4.2	3.4	59.9	16.5	1.4	4.9	206.8	230.5	25.7	201.5	28.2	2.8	2.7	0.25	7.7	281.5	55.7	105.4	
La Roya																							
OIS 0322	6.3	53.4	9.4	3.8 < L.D.		8.2	66.5	19.6	1.5	6.5	253.2	150.2	33.3	286.5	38.0	3.5	3.9	0.41	10.6	184.4	68.6	133.8	
Upper Monte Epomeo																							
MEGT 0318	5.1	39.9 < L.D.		1.9 < L.D.	< L.D.		54.8	16.7	1.4	4.9	292.8	673.0	24.7	213.3	28.9	2.6	3.0	0.31	6.3	199.4	52.9	98.1	
MEGT 0319	3.1	81.7	26.2	7.3	10.9	10.8	59.2	12.9	1.3	3.1	158.6	430.9	24.3	156.1	22.4	1.2	2.2	0.48	1.1	458.3	42.7	79.6	
MEGT 0328	5.5	40.8	19.2	2.3	9.1	6.9	54.6	16.1	1.2	5.1	322.1	591.5	24.0	194.0	28.3	1.9	3.4	0.40	6.9	184.0	47.0	93.3	
Lower Monte Epomeo																							
MEGT 0301	6.3	27.7 < L.D.		1.0 < L.D.	< L.D.		77.6	20.4	1.6	9.0	267.6	85.7	41.0	376.3	51.1	0.9	4.3	0.47	4.4	54.3	87.9	175.0	
OIS 0319	7.0	30.0 < L.D.		1.5 < L.D.	< L.D.		75.7	19.5	1.6	7.9	274.8	42.3	39.4	346.3	48.0	3.8	4.1	0.51	12.4	42.2	82.2	162.6	
OIS 0337	12.9	32.6	10.3	1.8			109.3	23.9	1.9	14.0	395.5	54.29	56.8	574.5	84.5	4.7	6.2	0.86	20.9	62.1	121.3	236.8	
OIS 0338	13.4	34.0	11.9	1.9			109.2	24.0	1.9	13.7	396.5	52.39	57.0	578.6	85.7	4.8	6.0	0.80	21.0	63.3	123.5	240.8	
OIS 0339	8.8	26.8	10.3	1.1			86.4	20.8	1.6	9.1	319.6	15.77	43.4	386.4	58.8	4.0	4.5	0.52	14.2	14.1	84.4	182.5	
OIS 0340	15.0	23.3	6.7	0.9			116.2	24.7	1.9	15.8	429.1	7.56	62.1	655.4	96.0	5.0	6.7	0.90	23.5	9.0	134.9	264.6	
OIS 0325	15.8	22.4 < L.D.		0.8 < L.D.	< L.D.		122.1	26.5	1.9	27.6	495.5	7.2	67.1	773.7	98.7	5.5	7.9	1.51	49.1	6.7	160.8	291.7	
OIS 0333	16.0	25.4 < L.D.		1.1 < L.D.		3.9	112.9	25.1	1.8	16.5	421.3	21.5	66.2	723.4	92.8	5.3	7.1	1.00	24.3	25.9	146.6	268.1	
OIS 0321	17.5	21.9 < L.D.		0.7 < L.D.		3.0	123.9	26.6	2.0	18.8	458.4	5.2	69.6	815.2	103.6	5.5	7.7	1.15	27.2	4.4	157.1	284.4	
Porticello																							
OIS 0320	14.3	24.3 < L.D.		1.0 < L.D.		3.1	105.5	23.7	1.8	14.2	371.6	17.3	61.5	623.3	81.3	5.1	6.5	0.79	20.5	14.4	131.3	244.5	
OIS 0316	13.8	24.3 < L.D.		0.7 < L.D.	< L.D.		108.5	24.8	1.8	15.0	393.6	8.9	62.6	642.6	85.0	5.4	6.6	0.88	21.7	7.2	134.9	252.8	
Tischello 60ka																							
OIS 0315	14.1	30.4 < L.D.		1.4 < L.D.	< L.D.		110.0	25.4	1.8	16.1	402.9	39.7	62.9	680.4	88.5	5.1	6.8	0.95	22.8	54.8	139.4	248.8	
OIS 0314	19.5	19.6 < L.D.		0.7 < L.D.	< L.D.		128.8	28.0	2.1	22.0	489.4	4.4	74.6	960.5	115.9	5.6	8.4	1.33	30.4	4.1	178.7	313.6	
OIS 0313	17.3	20.6 < L.D.		0.7 < L.D.	< L.D.		119.2	26.9	2.0	19.6	455.7	4.8	71.5	835.7	105.7	6.0	7.6	1.24	26.6	4.6	165.5	296.2	
OIS 0312	7.9	35.1 < L.D.		1.8 < L.D.	< L.D.		76.4	19.9	1.6	9.2	275.9	39.5	40.5	412.3	53.4	4.0	4.1	0.57	13.0	39.9	87.3	171.8	
OIS 0311	8.0	34.3 < L.D.		1.6 < L.D.	< L.D.		82.8	20.4	1.7	8.9	285.0	34.7	41.8	413.7	54.0	4.3	4.6	0.58	13.4	33.2	91.5	185.6	
OIS 0310	7.0	41.4 < L.D.		2.4 < L.D.	< L.D.		73.1	18.8	1.5	8.0	257.8	109.6	36.8	338.8	44.6	3.6	3.5	0.46	11.0	159.2	79.6	154.7	
OIS 0309	8.2	32.2 < L.D.		1.4	5.9 < L.D.		79.9	20.0	1.5	9.0	288.4	22.1	43.1	414.4	54.8	4.4	4.2	0.55	13.6	16.6	93.7	180.7	
OIS 0308	7.7	36.7	5.6	1.9 < L.D.		3.3	75.6	19.1	1.5	8.3	263.8	62.9	39.2	393.6	50.1	3.8	4.0	0.55	12.0	76.4	84.6	167.1	
Olummo 65																							
OIS 0318	7.9	39.0 < L.D.		6.3 < L.D.	< L.D.		84.0	21.0	1.6	8.5	287.2	56.3	42.1	410.5	53.7	3.8	4.2	0.52	13.3	68.0	93.0	181.7	
OIS 0317	7.8	43.5 < L.D.		2.4 < L.D.	< L.D.		78.6	20.0	1.6	8.0	267.4	98.2	38.8	365.0	48.3	3.2	3.9	0.51	11.5	137.3	83.3	160.5	
OIS 0307	8.1	34.5 < L.D.		1.6 < L.D.	< L.D.		79.3	19.8	1.7	8.7	275.4	30.8	40.9	406.4	51.8	4.0	4.2	0.57	12.7	27.8	87.8	171.0	
OIS 0306	12.8	32.3 < L.D.		1.5 < L.D.		3.7	99.1	23.2	1.8	13.5	353.8	28.4	58.0	637.1	77.6	4.7	5.8	0.94	19.0	27.8	132.7	235.2	
OIS 0305	19.2	24.7 < L.D.		0.9 < L.D.	< L.D.		130.7	27.2	2.1	21.7	468.7	9.9	80.4	945.2	117.1	5.8	8.1	1.32	28.7	8.4	185.2	331.1	
OIS 0304	20.7	22.7 < L.D.		0.8 < L.D.	< L.D.		138.3	29.3	2.1	23.9	505.2	8.3	84.3	1045.0	125.6	6.0	8.8	1.47	31.5	5.4	200.1	360.0	
OIS 0303	20.1	23.0 < L.D.		0.9 < L.D.	< L.D.		129.4	27.6	2.0	22.0	477.3	14.8	80.0	969.6	117.7	6.4	8.3	1.32	29.2	12.5	187.9	346.6	
OIS 0302	20.6	21.1 < L.D.		0.6 < L.D.		3.8	134.1	27.7	2.1	23.0	494.0	5.6	81.5	1058.0	122.7	5.8	8.8	1.51	30.8	4.5	202.9	354.8	
Mago 68																							
OIS 0301	20.0	22.1	5.6	0.7 < L.D.		5.6	132.0	27.6	2.1	22.0	473.5	11.9	80.4	103									

	Pr	Nd	Sm	Eu	Gd	Tb	Dy	Ho	Er	Tm	Yb	Lu	Hf	Ta	W	Pb	Th	U
Schiappone																		
MEGT 0315	14.9	52.9	9.5	1.5	18.4	1.1	6.2	1.2	3.4	0.5	3.2	0.50	7.0	2.8	4.5	35.9	19.8	5.9
MEGT 0317	12.0	43.1	7.8	1.6	16.5	0.9	4.9	1.0	2.8	0.4	2.5	0.39	5.4	2.1	3.5	31.9	14.9	4.5
MEGT 0316	14.2	50.4	9.0	1.6	18.3	1.0	5.7	1.1	3.2	0.4	3.0	0.47	6.4	2.6	4.1	35.4	18.1	5.4
MEGT 0311	14.9	52.0	9.3	1.5	18.1	1.1	6.0	1.1	3.1	0.5	3.3	0.51	7.3	2.8	4.6	32.5	21.9	6.1
MEGT 0310	15.6	55.2	10.0	1.6	18.3	1.2	6.3	1.2	3.3	0.5	3.4	0.52	6.9	2.7	4.4	37.0	19.9	6.3
MEGT 0309	13.3	48.2	8.9	1.8	16.9	1.0	5.5	1.0	2.7	0.4	2.8	0.42	5.4	2.1	3.4	32.7	14.7	4.7
MEGT 0308	15.4	54.4	9.8	1.5	18.3	1.1	6.2	1.1	3.2	0.5	3.4	0.52	7.0	2.8	4.6	36.4	19.9	6.3
MEGT 0307	15.5	54.6	9.8	1.5	18.9	1.1	6.3	1.2	3.3	0.5	3.4	0.53	7.1	2.8	4.5	35.9	20.0	5.9
MEGT 0306	15.4	55.3	9.9	1.6	7.7	1.2	6.2	1.1	3.2	0.5	3.2	0.48	6.8	2.7	4.5	34.8	18.9	5.9
MEGT 0314	16.1	56.1	10.0	1.4	19.7	1.2	6.5	1.3	3.6	0.5	3.5	0.54	7.7	3.1	5.0	39.7	22.4	6.6
MEGT 0313	16.2	56.8	10.2	1.4	7.8	1.2	6.5	1.2	3.5	0.5	3.5	0.55	7.8	3.1	4.9	37.9	22.2	6.9
MEGT 0312	15.8	55.1	9.9	1.3	19.4	1.2	6.4	1.2	3.5	0.5	3.5	0.54	7.7	3.1	4.9	39.1	22.1	6.6
MEGT 0305	14.3	51.4	9.5	1.7	17.7	1.1	6.0	1.1	3.0	0.4	2.9	0.46	6.5	2.5	4.3	33.2	17.4	5.3
Chiummano																		
OIS 0324	8.6	36.6	7.2	1.9	5.9	0.8	4.4	0.8	2.1	0.3	1.9	0.28	3.2	1.3	2.1	18.5	7.8	2.6
Capo grosso																		
OIS 0323	12.5	45.2	8.3	1.7	6.3	0.9	5.1	0.9	2.5	0.4	2.4	0.37	4.8	2.0	2.9	28.2	13.5	4.1
La Roya																		
OIS 0322	15.0	53.3	9.7	1.6	19.6	1.1	6.2	1.1	3.1	0.5	3.1	0.47	6.3	2.6	4.0	34.2	18.5	5.4
Upper Monte Epomeo																		
MEGT 0318	11.3	40.8	7.4	1.6	5.7	0.8	4.7	0.9	2.4	0.3	2.3	0.35	5.0	2.0	3.0	30.6	13.2	4.2
MEGT 0319	9.5	34.6	6.5	1.5	5.3	0.8	4.3	0.8	2.2	0.3	2.1	0.33	3.8	1.5	2.6	28.9	9.4	3.5
MEGT 0328	9.8	39.2	7.0	1.6	5.5	0.8	4.4	0.8	2.2	0.3	2.2	0.34	4.6	1.9	2.4	29.7	12.7	4.0
Lower Monte Epomeo																		
MEGT 0301	19.6	69.4	12.4	1.3	9.5	1.4	7.6	1.4	3.9	0.6	3.8	0.57	7.8	3.3	1.7	36.9	22.4	6.7
OIS 0319	18.5	65.3	11.8	1.4	19.5	1.4	7.3	1.3	3.7	0.5	3.6	0.55	7.4	3.3	4.0	42.0	22.1	6.4
OIS 0337	25.6	88.2	15.3	1.3	11.6	1.8	10.0	1.9	5.4	0.8	5.6	0.86	12.6	5.0	7.1	52.5	35.9	11.5
OIS 0338	25.9	89.5	15.6	1.3	11.7	1.8	10.1	1.9	5.5	0.8	5.6	0.86	12.6	5.1	7.3	48.7	36.3	11.7
OIS 0339	20.6	73.7	12.9	1.3	9.7	1.5	8.0	1.5	4.1	0.6	4.0	0.61	8.4	3.6	5.9	39.8	23.9	7.6
OIS 0340	27.6	93.9	16.1	1.1	12.2	1.9	10.7	2.0	5.9	0.9	6.2	0.97	14.3	5.5	7.7	52.6	41.5	13.2
OIS 0325	30.6	100.0	17.1	1.1	13.1	2.1	11.8	2.3	6.8	1.1	7.2	1.13	16.7	6.2	6.6	89.5	50.3	14.8
OIS 0333	28.4	94.0	16.1	1.1	25.1	1.9	11.3	2.1	6.2	1.0	6.6	1.06	16.1	6.0	6.5	50.2	47.1	13.8
OIS 0321	29.5	96.0	16.1	0.9	26.6	2.0	11.3	2.2	6.5	1.0	7.1	1.13	16.7	6.1	6.6	59.6	52.3	15.3
Porticello																		
OIS 0320	27.1	91.9	16.3	1.2	23.7	1.9	10.9	2.1	5.8	0.9	6.0	0.94	13.0	5.2	6.1	51.4	40.2	11.9
OIS 0316	27.5	94.0	16.5	1.1	24.8	2.0	10.9	2.0	5.9	0.9	6.1	0.94	13.5	5.5	6.1	52.8	41.6	12.2
Tischietto 60ka																		
OIS 0315	27.0	89.8	15.5	1.2	25.4	1.8	10.4	2.0	5.8	0.9	6.1	0.96	13.8	5.2	5.8	52.9	43.5	12.7
OIS 0314	31.6	99.9	16.4	0.9	12.8	2.1	12.1	2.4	7.4	1.2	8.3	1.35	20.2	6.7	7.2	66.2	62.3	18.1
OIS 0313	30.5	99.7	16.6	1.0	12.8	2.0	11.7	2.3	6.9	1.1	7.5	1.23	17.6	6.3	7.1	60.8	54.6	15.7
OIS 0312	18.6	64.0	11.3	1.3	8.6	1.3	7.4	1.4	3.9	0.6	4.0	0.64	8.8	3.6	4.6	41.6	26.3	7.3
OIS 0311	19.6	67.6	12.0	1.5	9.1	1.4	7.7	1.4	4.1	0.6	4.2	0.65	8.8	3.5	4.5	38.2	26.8	8.0
OIS 0310	17.2	60.4	10.7	1.6	8.3	1.2	6.8	1.3	3.5	0.5	3.6	0.55	7.2	3.0	3.9	34.6	22.2	6.3
OIS 0309	20.0	69.3	12.1	1.5	9.3	1.4	7.9	1.5	4.2	0.6	4.2	0.67	8.9	3.6	4.9	38.7	27.2	7.9
OIS 0308	18.3	63.6	11.3	1.5	19.1	1.3	7.1	1.3	3.8	0.6	3.9	0.59	8.3	3.3	4.1	36.7	24.3	6.9
Olummo 65																		
OIS 0318	20.0	68.6	12.2	1.7	9.3	1.4	7.7	1.4	4.2	0.6	4.1	0.67	8.8	3.6	4.2	38.5	26.4	7.4
OIS 0317	17.7	62.3	11.1	1.6	20.0	1.3	7.0	1.3	3.7	0.5	3.7	0.57	7.6	3.1	3.7	35.3	23.9	6.6
OIS 0307	18.9	65.6	11.6	1.4	19.8	1.3	7.4	1.4	3.9	0.6	4.0	0.61	8.3	3.3	4.2	36.6	24.9	7.2
OIS 0306	25.5	85.5	14.7	1.3	23.2	1.7	9.9	1.9	5.5	0.8	5.8	0.91	12.9	4.7	5.2	46.7	39.1	11.1
OIS 0305	34.1	110.4	18.6	1.1	14.5	2.3	13.3	2.6	7.8	1.2	8.6	1.37	19.7	6.8	6.8	68.4	66.5	18.3
OIS 0304	36.0	113.4	18.7	1.0	14.5	2.3	13.8	2.7	8.2	1.3	9.2	1.47	21.9	7.1	7.2	69.1	74.7	20.8
OIS 0303	34.2	109.4	18.1	1.0	14.3	2.2	13.0	2.6	7.8	1.2	8.7	1.37	20.3	6.8	7.7	67.7	69.3	19.0
OIS 0302	35.3	111.6	18.4	1.0	27.7	2.3	13.1	2.6	7.8	1.3	9.0	1.43	21.9	7.0	7.1	68.1	72.5	20.9
Mago 68																		
OIS 0301	34.6	110.6	18.1	1.0	27.6	2.3	13.0	2.5	7.6	1.2	8.7	1.36	20.7	6.7	7.0	66.6	69.6	18.5
Sant'angelo 70																		
OIS 0332	36.6	115.7	19.0	1.0	29.6	2.4	14.0	2.7	8.2	1.3	9.3	1.49	23.5	7.5	3.9	67.2	76.7	18.8
OIS 0331	35.8	113.7	18.6	1.0	29.6	2.3	13.6	2.7	8.0	1.3	9.1	1.46	22.9	7.3	3.2	64.9	73.4	18.0
OIS 0330	29.7	97.6	16.4	1.0	26.4	2.0	11.5	2.2	6.4	1.0	7.0	1.11	16.9	6.2	6.6	59.4	50.9	14.8
OIS 0329	25.5	85.1	14.5	1.6	22.5	1.7	9.6	1.8	5.2	0.8	5.7	0.88	12.9	4.7	5.2	50.7	44.7	12.4
OIS 0328	29.1	95.0	16.2	1.4	12.3	1.9	10.9	2.1	6.2	1.0	6.9	1.09	16.4	5.6	5.9	49.0	55.2	16.1
OIS 0327	31.4	101.6	17.3	1.5	13.2	2.1	11.8	2.2	6.8	1.1	7.2	1.17	17.5	6.0	6.4	61.9	59.2	16.9
OIS 0326	30.3	98.9	16.6	1.3	24.8	2.0	11.6	2.2	6.4	1.0	7.2	1.13	16.9	5.9	6.3	56.3	59.5	16.7
Barano																		
OIS 0334	20.9	72.3	12.8	1.7	9.7	1.5	8.0	1.5	4.3	0.6	4.2	0.64	8.5	3.4	3.4	44.1	26.1	6.0

	87Sr/86Sr	2s	87Sr/86Sr	2s	87Sr/86Sr	2s	143Nd/142Nd	2s
Schiappone								
MEGT 0315			0.706741	0.000006				
MEGT 0317	0.706748	0.000005						
MEGT 0316	0.706754	0.000007					0.512527	0.000004
MEGT 0311			0.706779	0.000006				
MEGT 0310	0.706798	0.000008						
MEGT 0309			0.70675	0.000006				
MEGT 0308								
MEGT 0307			0.706749	0.000006				
MEGT 0306	0.706773	0.000007						
MEGT 0314			0.706757	0.000006			0.512529	0.000005
MEGT 0313								
MEGT 0312	0.706761	0.000008					0.51253	0.000005
MEGT 0305			0.706752	0.000006				
Chiummano								
OIS 0324			0.706691	0.000006	0.706668	0.000007	0.512534	0.000006
Capo grosso								
OIS 0323		0.000005	0.706686	0.000006				
La Roya								
OIS 0322		0.000009	0.706732	0.000006				
Upper Monte Epomeo								
MEGT 0318			0.706907	0.000006			0.512527	0.000004
MEGT 0319							0.512537	0.000005
MEGT 0328			0.706818	0.000006			0.512541	0.000001
Lower Monte Epomeo								
MEGT 0301			0.706898	0.000006			0.512535	0.000015
OIS 0319			0.706764	0.000006			0.512541	0.000005
OIS 0337			0.706779	0.000007				
OIS 0338			0.706773	0.000006				
OIS 0339			0.706765	0.000006				
OIS 0340			0.70681	0.000006			0.512537	0.000004
OIS 0325			0.706848	0.000006			0.512542	0.000004
OIS 0333							0.512542	0.000004
OIS 0321			0.706753	0.000008			0.512534	0.000005
Porticello								
OIS 0320	0.706784	0.000007					0.512539	0.000005
OIS 0316	0.706752	0.000007						
Tischietto 60ka								
OIS 0315			0.706732	0.000006			0.512536	0.000006
OIS 0314			0.706815	0.000006				
OIS 0313			0.706878	0.000006	0.706842	0.000007		
OIS 0312			0.706452	0.000006				
OIS 0311			0.706446	0.000006			0.512547	0.000004
OIS 0310			0.706441	0.000006			0.51255	0.000005
OIS 0309								
OIS 0308			0.706449	0.000006				
Olummo 65								
OIS 0318			0.706416	0.000006				
OIS 0317	0.706468	0.000007						
OIS 0307								
OIS 0306	0.706421	0.000007					0.512547	0.000005
OIS 0305			0.70646	0.000007			0.512529	0.000004
OIS 0304							0.51254	0.000003
OIS 0303			0.706519	0.000006			0.512541	0.000005
OIS 0302			0.706569	0.000006				
Mago 68								
OIS 0301			0.706537	0.000006			0.512536	0.000005
Sant'angelo 70								
OIS 0332			0.706626	0.000006			0.512544	0.000005
OIS 0331			0.706557	0.000006			0.512538	0.000004
OIS 0330			0.706612	0.000007			0.512537	0.000006
OIS 0329	0.706653	0.000007						
OIS 0328	0.706642	0.000006					0.512545	0.000004
OIS 0327	0.706638	0.000008	0.706614	0.000006			0.512545	0.000006
OIS 0326			0.706635	0.000006			0.512547	0.000006
Barano								
OIS 0334	0.70642	0.000007					0.512553	0.000005

* Age corrected isotope ratios

** Different aliquot of feldspar crystals

Table 2 – Summary of petrographic features of 75-50 ka Ischia volcanic rocks

Unit	TAS Classification	Phenocrysts		Groundmass	
		type and relative abundance of minerals	P.I. vol.%	texture	additional minerals
Schiappone	LT/TR	alk-fd > pl, cpx > bt, mt ± ol	5–15	vitric, microcrystalline	
Chiummano	LT	alk-fd > pl, cpx > bt, ol, mt	25	hypocrystalline	
Capo Grosso	TR	alk-fd > pl > cpx > bt > mt	15	hypocrystalline	
La Roja	TR	alk-fd > pl >> cpx, bt, mt	12	hypocrystalline	
Upper MEGT	TR	alk-fd > pl ± cpx > bt > mt	15–36	felty, perlitic	ap
Lower MEGT	TR/PH	alk-fd >> cpx, bt, pl > mt ± sph	13–41	vitric, felty, fluidal	ap
Porticello	TR/PH	alk-fd >> cpx ± mt	2–4	vitric	
Tisichiello	TR/PH	alk-fd >> cpx, bt > mt	5–7	vitric	
Olummo	TR/PH	alk-fd >> bt > cpx ± pl > mt	5–15	vitric, microcrystalline	
Mago	PH	alk-fd	2–3	vitric	
Sant'Angelo	PH	alk-fd >> cpx, bt ± pl, mt, sph, ne	5–20	vitric, microcrystalline	amph
Barano	TR	alk-fd >> cpx, bt > pl > mt	15	felty, microcrystalline	

Key for mineral names: alk-fd = alkali-feldspar; pl = plagioclase; bt = biotite; cpx = clinopyroxene; mt = titano-magnetite; ol = olivine; amph = amphibole; sph = sphene; ne = nepheline; ap = apatite. P.I. = porphyricity index

Table 3 - Summary of data and results of fractional crystallization modelling

From Chiummano latite (OIS 0324) to the TiO₂-poor Schiappone trachite (MEGT 0312)

OXIDE (wt.%)	parent magma	daughter magma	subtracted phases					daughter magma	Σr^2	amount (wt.%) of subtracted phases		total amount (wt.%) of subtracted phases [#]
	observed	observed	Cpx	Pl	Bt	Mt	Ap	calculated				
SiO ₂	55.71	62.65	51.09	52.65	41.24	0.06	0.53	62.72	0.25	Cpx	36.94	43.75
TiO ₂	0.80	0.42	0.64	0.07	3.83	7.57		0.37		Pl	35.39	
Al ₂ O ₃	17.14	18.92	3.88	29.66	11.99	2.59	0.01	18.99		Bt	22.05	
FeO _{tot}	5.18	2.46	5.04	0.64	13.87	86.52	0.17	2.53		Mt	3.89	
MnO	0.14	0.14	0.08		0.90	1.21	0.10	0.08		Ap	1.72	
MgO	4.54	0.57	15.75	0.05	17.38	2.04	0.27	0.52				
CaO	7.12	1.53	23.39	12.46		0.02	59.61	1.63				
Na ₂ O	3.44	5.56	0.13	3.95	0.84		0.18	5.16				
K ₂ O	5.58	7.65		0.53	9.94		0.02	7.89				
P ₂ O ₅	0.36	0.10			0.01		39.10	0.11				
TOT	100.00	100.00	100.00	100.00	100.00	100.00	100.00	100.00				

From Schiappone latite (OIS 0324) to the TiO₂-rich phonolite (glass of sample OIS 0320*)

	parent magma	daughter magma	subtracted phases			daughter magma	Σr^2	amount (wt.%) of subtracted phases		total amount (wt.%) of subtracted phases [#]
	observed	observed	A-fd	Pl	Amp	calculated				
SiO ₂	62.65	61.04	65.47	59.17	44.94	61.35	0.39	A-fd	76.78	62.58
TiO ₂	0.42	0.61	0.16	0.00	2.61	0.62		Pl	16.94	
Al ₂ O ₃	18.92	18.89	18.44	24.89	7.58	18.95		Amp	6.28	
FeO _{tot}	2.46	3.04	0.58	0.55	18.13	3.30				
MnO	0.14	0.28	0.00	0.00	2.06	0.24				
MgO	0.57	0.32	0.02	0.04	9.66	0.38				
CaO	1.53	1.10	0.23	7.41	10.00	0.93				
Na ₂ O	5.56	8.74	3.56	6.24	3.53	8.52				
K ₂ O	7.65	5.93	11.54	1.70	1.48	5.58				
P ₂ O ₅	0.10	0.06				0.14				
TOT	100.00	100.00	100.00	100.00	100.00	100.00				

* from Tomlinson et al., in preparation. Σr^2 = sum of the squares of the residuals. [#] relative to initial magma. Key for the names of minerals: Cpx = clinopyroxene; Pl = plagioclase; Bt = biotite; Mt = magnetite; Ap = apatite; A-fd = alkali-feldspar; Amp = amphibole.

Table 4. Constraints and results of the geochemical modelling (see text)

	Step 4	Chiummano OIS 0324	Schiappone MEGT 0308.	Schiappone MEGT 0312	S. Angelo OIS 0329	MELTS Step 1 (from OIS 0324 to MEGT 0308)	MELTS Step 2 (from MEGT 0308 to MEGT 0312)	MELTS Step 3 (late phonolite)	MELTS (residual liquid) ^(^^)
SiO ₂		55.39	61.25	62.64	62.00	60.61	62.09	61.14	56.92
TiO ₂		0.79	0.47	0.42	0.70	0.57	0.53	1.05	1.73
Al ₂ O ₃		17.04	18.64	18.91	18.80	20.22	19.77	18.77	17.37
FeO _{tot}		5.73	2.92	2.46	2.90	1.45	1.01	1.13	0.88
MnO		0.14	0.13	0.14	0.30	0.19	0.18	0.43	2.17
MgO		4.51	1.22	0.57	0.30	0.82	0.76	1.21	0.62
CaO		7.08	2.31	1.53	1.26	3.22	2.50	2.67	1.94
Na ₂ O		3.42	5.36	5.56	7.40	4.48	5.46	6.46	12.81
K ₂ O		5.55	7.56	7.65	6.40	7.92	7.20	6.15	4.58
P ₂ O ₅		0.36	0.13	0.10	n.a.	0.52	0.50	0.98	0.97
TOT		100.00	100.00	100.00	100.00	100.00	100.00	100.00	100.00
Summary of mineral geothermobarometry					/				
<i>Biotite</i>									
			0.27	0.18					
			0.47	1.28					
			0.088	0.118					
			0.71	0.93					
			0.288	0.0072					
			0.0045	0.0005					
<i>Sanidine</i>									
			0.45	0.68					
<i>Magnetite</i>									
			0.71	0.71					

T (°C)	930	930
fH ₂ O (bar)	668	498
fHF (bar)	0.4	0.07
fHCl (bar)	335	18
logfO ₂	NNO+0.75	NNO+1.44
H ₂ O (#)	2.90	2.40
Ptot(MPa) (*)	100	52
Ptot (MPa) (**)	~160	~100
Ptot (av.estimate)	130	75

Summary of
MELTS runs

Temperature (°C)

Initial	1200	930	930	930
Final	930	930	930	910

Pressure (MPa)

Initial	200	100	100	60
Final	130	100	60 (@)	10

H ₂ O (wt%)	2.5	3.46 (§)	3.34	2.910	1.47
------------------------	-----	----------	------	-------	------

Redox state

ΔFMQ	+1	+2	+2	+2
ΔNNO	+0.45	+1.43	+1.43	+1.43

<i>Liquid (grams)</i>	72.02	103.41	40.68	3.24
-----------------------	-------	--------	-------	------

Fractionated Phases (grams)

Olivine (Fo ₈₃)	2.46			
Olivine (Fo ₆₇ Teph ₂₅ Fa ₈)				0.47
Cpx (Di ₅₅)	18.54			
Cpx ???				0.61
Plagioclase (An ₅₉)	4.77			
Plagioclase (Ab ₅₇ Or ₃₁ An ₁₂)				46.85
Feldspar (Or ₆₇)		62.56		
Feldspar (Or ₆₉)		13.40		
Biotite			0.47	0.47
Feldspar (Ab ₆₀ An ₃₀ Or ₁₀)			13.59	

Feldspar (Ab ₃₇ An ₅ Or ₅₈)				42.07
Feldspar (Or ₆₀)			42.07	
Spinel		0.62	0.83	1.72
Apatite			0.22	1.05
Water				
<i>Solids</i> (grams)				
Biotite	0.17		>0.0	
Plagioclase (An ₅₃)	1.61			
Feldspar (Ab ₆₂ An ₂₆ Or ₁₂)			>0.0	
Spinel	0.15		>0.0	
Feldspar (Or ₆₇)		8.12		
Nepheline (Na-Neph ₆₀)				0.04
Water			2.13	
<i>Assimilant</i>				
Phase added		50 wt% Na-feldspar (Ab ₇₀ Or ₃₀)		
Phase added		50 wt% K-feldspar (Ab ₁₀ Or ₉₀)		
Temperature		600°C		
Pressure		100 Mpa		
Amount added (grams):		80		
Total mass of the system	100	180	100	100

(*) CO₂ was not considered.

(**) The possible presence of CO₂ was considered.

(#) Water (in wt%) from application of the saturation model of Papale et al. (2006).

(§) Note that in this step MELTS runned under water-undersaturated conditions.

(@) Nepheline precipitated in the subsequent step, by decompression to 10 MPa and cooling down to 910°C.

(^^) This step is the prosecution of the previous one. It is put here to show the consequences of MELTS calculation on extreme fractionations: note the unreasonably high TiO₂, MnO and P₂O₅ values.

Table 5: Parameters the EC-AFC model.

(a)	
Model parameters	
T _{lm}	1250 °C

T_{m0}	1250 °C
T_{la}	950 °C
T_{a0}	400 °C
T_s	700 °C
C_{pm}	1484 J/kg K
C_{pa}	1388 J/kg K
h_{cry}	396000 J/kg
h_{fus}	270000 J/kg
T_{eq}	950 °C

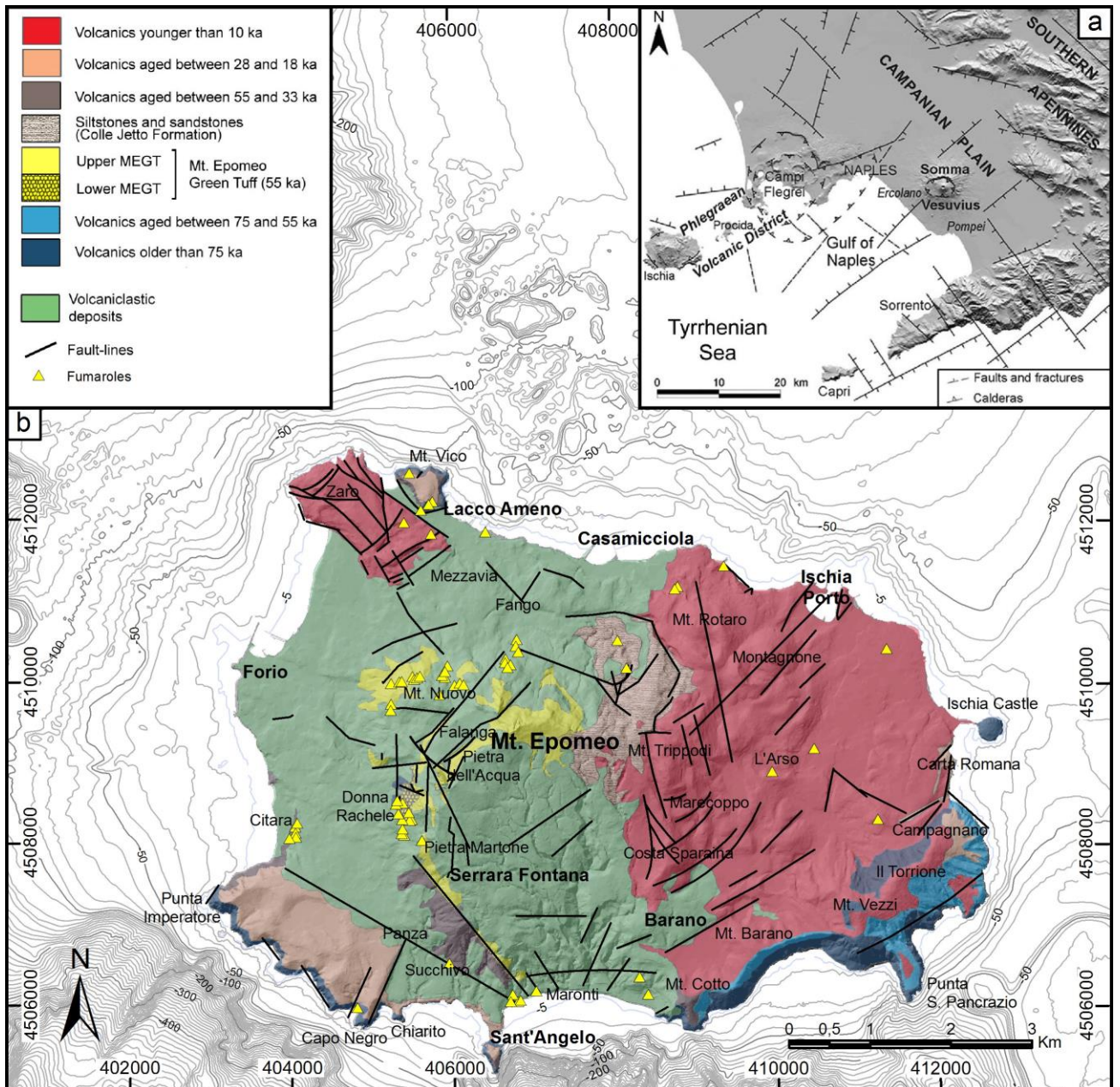
(b) Endmember compositions

Element	Sr (ppm)	Nd (ppm)	Th (ppm)
Concentration in magma	548	37	8
Bulk D_0	3.5	0.05	0.0001
Concentration in assimilant	298	36	5
Bulk D_0	0.02	0.04	0.0001
Isotope	$^{87}\text{Sr}/^{86}\text{Sr}$	$^{143}\text{Nd}/^{144}\text{Nd}$	Th (ppm)
Isotope ratio: magma	0.706420	0.512547	
Isotope ratio: assimilant	0.7140	0.5122	
Sr, Nd, Pb, Th of the contaminated magma (ppm)	356	46	14
Isotope ratio of the contaminated magma	0.706838	0.512537	

T_{eq} equilibration temperature	$C_{p,m}$ magma isobaric specific heat capacity
T_{lm} magma liquidus temperature	$C_{p,a}$ assimilant isobaric specific heat capacity
T_{m0} initial magma temperature	T_{la} wallrock liquidus temperature
h_{cry} crystallisation temperature	h_{fus} fusion enthalpy
T_{a0} initial wall rock temperature	T_s wall rock solidus temperature
D_0 distribution coefficient	

The distribution coefficients of Sr, Nd and Th for the evolving magma were assumed equal to 3.5, 0.05, 0.6 and 0.0001, respectively, in agreement with the compatible behaviour of Sr and incompatible behaviour of Nd and Th during magma evolution. We assumed an initial temperature of 1250 °C (T_{m0}) for the poorly differentiated magma, in line with the experimental estimates of [Cannatelli et al. \(2007\)](#). An initial temperature (T_{a0}) of 400 °C was assigned to the crust. The liquidus temperature (T_{la}) of the crust was assumed equal to 950 °C, its solidus temperature (T_s) equal to 700 °C (e.g., [Wyllie, 1977](#)). The equilibration temperature (T_{eq}) was assumed equal to 950°C. At that temperature, the modeled daughter magma has Sr = 356 ppm, Nd = 46 and Th = 14

ppm, $^{87}\text{Sr}/^{86}\text{Sr} = 0.706838$ and $^{143}\text{Nd}/^{144}\text{Nd} = 0.512537$. The modeled daughter magma has geochemical and Sr isotopic composition close to that of the trachytic Schiappone magmas.



Unit	Description	Lower contact	Upper contact	Distribution	Interpretation
Schiappono Tephra	Member A is a >25 m thick pumice fall deposit exhibiting cm-thick horizons of pink-ash-coated pumice lapilli, a <30 cm of stratified, cross-stratified lithic-rich ignimbrite with accretionary lapilli-bearing ash beds; upper >3 m comprise a thick bedded pumice breccia with a welded top. Member B is an >60 m thick massive or diffuse bedded ignimbrite with occasional metre-scale dune bedforms.	Overlies a palaeosol in MEGT, Chiummano tephra.	Passes up into a palaeosol; top often eroded. Passes up into a palaeosol.	Monte Cotto to Carta Romana; also Sant'Angelo, Punta Imperatore, Monte Vico and Procida Island	Member A: major explosive (Plinian?) eruption with fallout from unsteady eruption column and short-lived pyroclastic density currents (PDCs). Member B: PDC deposits.
	Succession of bedded and cross-stratified lithic-rich ignimbrites up to 7 m thick and thin accretionary lapilli-bearing tuffs; contains banded and homogeneous pale-grey and black basaltic-trachyandesite pumice and scoria and abundant lithic clasts; at Monte Cotto, it is a coarse pumice and scoria fall deposit; at Punta Imperatore it is a < 12 cm thick lithic-rich ash layer.	Overlies a palaeosol in the La Roia, MEGT and older units.	Passes up into a palaeosol.	Grotta di Terra to Monte Cotto; Sant'Angelo; Punta Imperatore	Medial and distal deposits of a maar volcano.
Chiummano Tephra	50 cm-thick normally-graded pumice fall deposit.	Unconformably overlies the >150 ka BP deposits	Passes up into a palaeosol.	Sant'Angelo to Punta Imperatore	Fallout from a Plinian/Subplinian eruption column.
La Roia Tephra	>40 m thick diffuse-bedded ignimbrite with porphyritic pumice and dense banded porphyritic scoria clasts, and abundant hydrothermally altered lithic clasts, exhibits metre-thick beds of angular clast-supported pumice and scoria.	overlies a palaeosol in the MEGT.	Passes up into a palaeosol.	Monte Cotto	PDC deposits from an explosive eruption.
Capo Grosso Tephra	Intracaldera - two ignimbrite flow-units: >70 m thick lower MEGT composed of <20 m thick lithic breccia overlain by ~50 m thick massive ignimbrite with dense spatter, pumice in a crystal-rich matrix; >200 m thick upper MEGT is a stratified and massive ignimbrite. Extracaldera - basal 7 m thick pumice fall deposit; 4 m thick non-to weakly-welded and diffuse-bedded ignimbrite; and a widespread 12 m thick lithic breccia.	Base not exposed; overlies marine volcanoclastic sandstones and conglomerates; upper MEGT overlies reworked lower MEGT; overlies palaeosol in extracaldera localities.	Unconformably overlain by marine volcanoclastic siltstones and sandstones (Colle letto Formation, Vezzoli 1988).	Monte Vezzi to Carta Romana; Sant'Angelo; Punta Imperatore; Monte Vico; Procida Island and Monte di Procida (SW Campi Flegrei)	Plinian eruption with caldera collapse; Extracaldera deposits record fallout from Plinian eruption column; intracaldera deposits record widespread and sustained PDCs. Lithic breccias record caldera collapse.
Monte Epomeo Green Tuff	3.5 m pumice fall deposit with thin orange-brown lapilli-tuff layers containing carbonised vegetation.	Overlies an unconformity and palaeosol in the Tischiello Tephra.	Passes up into a brown palaeosol.	Monte Vezzi to Carta Romana	Fall out from an unsteady (?Subplinian) eruption column; short-lived PDCs
Porticello Tephra	7 m thick bedded pumice fall deposit; bedding defined by changes in the pumice vesicularity, grain size, grading and lithic lapilli abundance; cm to dm thick ash layers and diffuse-stratified lapilli-tuff layers with carbonised vegetation.	Overlies an unconformity and palaeosol in the Olummo Tephra.	Passes up into a brown palaeosol; major unconformity and volcanoclastic sediments.	Monte Vezzi to Carta Romana	Fall out from an unsteady (?Subplinian) eruption column; short-lived PDCs
Tischiello Tephra	<6 m thick diffuse-bedded pumice fall deposit with thin ash layers overlain by a 2 m thick breccia; bedding defined by grain size variations, juvenile obsidian, banded pumice and scoria and lithic lapilli layers; contains diffuse-stratified lapilli-tuff layers with carbonised vegetation; breccia comprises clast-supported dense phonolite lapilli and subordinate pumice lapilli in a fines-depleted crystal-lithic ash matrix.	Unconformably overlies the palaeosol in the top of the Mago Tephra.	Passes up into a palaeosol.	Monte Vezzi to Carta Romana	Fall out from an unsteady (?Subplinian) eruption column followed by lava dome growth and generation of block-and-ash flows.
Olummo Tephra					
Mago Tephra	~ 60 cm thick pumice fall deposit.	Overlies a scoria breccia of the 74 ka Parata Formation.	Passes up into a palaeosol.	Grotta di Terra	Fallout from unsteady eruption column
Sant'Angelo Tephra	Lower unit comprises interbedded pumice fall deposits and diffuse bedded ignimbrites with imbricated and incipiently welded pumice and scoria lapilli and blocks; upper unit comprises two mononict poorly sorted lava breccias separated by a 1 m thick pumice fall deposit.	Overlies a palaeosol on lava dome (~100 ka, Gillot et al. 1982); not seen in contact with other pre-MEGT deposits; relative age not fully established.	unconformably overlain by extracaldera MEGT.	Sant'Angelo	Products of a small volcano characterised by lava dome extrusion and small-volume explosive activity, that showered pumice over the south of the island and generated small PDCs and block-and-ash flows.

20 m

lava > 75 ka

